Table 2

Relationship of CT Features with Prognostic Factors

	Lymphatic Invasion ($n = 145$)			Pleural Invasion ($n = 51$)		
Logistic Regression Analysis	No. of Tumors	Odds Ratio	*P* Value	No. of Tumors	Odds Ratio	*P* Value
Univariate analysis						
Visual classification						
Pure GGN	15	1.96 (0.24, 15.97)	.49	1	ND*	ND*
Solid	130	...	...	50	ND*	ND*
Software classification						
Pure GGN	15	1.96 (0.24, 15.97)	.49	0	ND*	ND*
Solid	130	...	...	51	ND*	ND*
Longest diameter of tumor						
<18 mm	94	1.01 (0.35, 2.90)	.99	27	0.95 (0.27, 3.37)	.94
≥18 mm	51	...	...	24	...	...
Longest diameter of solid component						
<9.9 mm	81	2.17 (0.67, 6.99)	.19	21	3.00 (0.71, 12.65)	.13
≥9.9 mm	64	...	...	30	...	...
Solid proportion						
<78%	90	2.04 (0.65, 6.43)	.22	24	4.12 (0.98, 17.38)	.05
≥78%	55	...	...	27	...	...
Total tumor volume						
<1.9 cm^3	84	0.96 (0.34, 2.68)	.94	21	1.16 (0.32, 4.23)	.81
≥1.9 cm^3	61	...	...	30	...	...
Solid volume						
<1.5 cm^3	101	1.29 (0.45, 3.75)	.64	26	1.30 (0.37, 4.58)	.69
≥1.5 cm^3	44	...	...	25	...	...
Percentage of solid volume						
<63%	88	2.46 (0.88, 6.90)	.08	23	6.03 (1.58, 22.98)	.01
≥63%	57	...	...	28	...	...
Multiple analysis (by stepwise method)						
Percentage of solid volume						
<63%	88	ND	ND	23	6.03 (1.58, 22.98)	.01
≥63%	57	ND	ND	28	...	...

Note.—Data in parentheses are 95% confidence intervals. *P* values less than .05 indicated statistical significance. ND = no data.

* Statistical analysis for association with pleural invasion could not be performed because of a small number of juxtapleural nodules in GGN division.

1.9 cm^3; solid volume, 1.5 cm^3; and solid volume, 63%.

Results for association of eight CT features with two prognostic factors are summarized in Table 2. Statistical analysis was performed to examine associations with lymphatic invasion in 145 cases and pleural invasion in 51 cases; none of the resected tumors were found by using pathologic examination to have vascular invasion. Statistical analysis for examining the association with pleural invasion was performed only for those tumors that were juxtapleural in location. None of the eight CT features were found to be of use in examination of presence of lymphatic invasion. Univariate and multiple logistic regression analyses revealed that percentage of solid volume of 63% or greater was of significant use in examination of presence of pleural invasion (odds ratio, 6.03 [95% confidence interval: 1.58, 22.98]; $P = .01$).

Relationship with Recurrence and Survival

During a 7-year follow-up period, 22 patients experienced disease recurrence, and there were seven associated cancer-related deaths. All cases of recurrence and death occurred in patients with tumors classified as part-solid GGN ($n = 6$) or solid ($n = 16$); none occurred in patients with tumors classified as GGN.

Results for relationship of eight CT features with disease-free survival and overall survival are summarized in Table 3. Multiple analyses showed that percentage of solid volume of 63% or greater was a significant indicator for lower disease-free survival ($P < .001$). Both univariate and multiple analyses showed that solid volume of 1.5 cm^3 or greater and three-dimensional percentage of solid of 63% or greater were significant ($P < .05$) indicators for lower overall survival. Figures 4 and 5 show the lower disease-free and

Table 3

Association of CT Features with Survival

Cox Proportional Hazards Regression Analysis	No. of Tumors	Disease-free Survival		Overall Survival	
		Hazard Ratio	*P* Value	Hazard Ratio	*P* Value
Univariate analysis					
Visual classification					
Pure GGN	15	310644 (0.00, 3.48×10^{198})	.097	113504 (0.00, 5.23×10^{198})	.375
Solid	130	...	...	...	...
Software classification					
Pure GGN	15	310644 (0.00, 3.48×10^{198})	.097	113504 (0.00, 5.23×10^{198})	.375
Solid	130	...	...	...	...
Longest diameter of tumor					
<18 mm	94	2.89 (1.19, 6.98)	.012	2.65 (0.57, 12.22)	.207
≥18 mm	51	...	...	...	...
Longest diameter of solid component					
<9.9 mm	81	9.23 (2.74, 31.02)	<.001	7.93 (0.96, 65.19)	.055
≥9.9 mm	64	...	...	...	...
Solid proportion					
<78%	90	8.12 (2.76, 23.87)	<.001	4.32 (0.84, 22.08)	.080
≥78%	55	...	...	...	...
Total tumor volume					
<1.9 cm^3	84	4.57 (1.96, 11.43)	.001	3.81 (0.84, 12.31)	.086
≥1.9 cm^3	61	...	...	...	...
Solid volume					
<1.5 cm^3	101	7.17 (2.79, 18.35)	<.001	5.90 (1.17, 29.80)	.016
≥1.5 cm^3	44	...	...	...	...
Percentage of solid volume					
<63%	88	8.18 (2.80, 18.35)	<.001	9.58 (2.09, 43.91)	.01
≥63%	57	...	...	...	...
Multiple analysis (by stepwise method)					
Solid volume					
<1.5 cm^3	101	...	...	5.92 (1.17, 30.33)	.034
≥1.5 cm^3	44	...	...	...	...
Percentage of solid volume					
<63%	88	18.45 (4.34, 78.49)	<.001	9.60 (1.17, 78.91)	.036
≥63%	57	...	...	...	...

Note.—Data in parentheses are 95% confidence intervals. *P* values less than .05 indicate statistical significance.

overall survival for patients with solid volume of 1.5 cm^3 or greater (7-year disease-free survival and overall survival rates, 58.6% and 85.1%, respectively) and percentage of solid volume of 63% or greater (7-year disease-free survival and overall survival rates, 60.1% and 86.3%, respectively) compared with patients with solid volume less than 1.5 cm^3 (7-year disease-free survival and overall survival rates, 92.4% and 98.0%, respectively; $P \leq .015$) and percentage of solid volume of less than 63% (7-year disease-free survival and overall survival rates, 96.3% and 98.9%, respectively; $P \leq .01$).

Table 4 shows quantitative measurements, types of resection performed, and sites of recurrence in 22 patients with recurrence and death. Of the eight smallest tumors that were less than 15.5 mm in longest diameter, six tumors (75%) had solid volume of less than 1.5 cm^3 and one (13%) had percent solid volume of less than 63%. A 27-mm part-solid tumor that resulted in patient death had multiple foci of solid components with measured solid volume of 2.77 cm^3 and percentage of solid volume of 29.8% (Fig 6). Ten patients with recurrent disease presented with a solitary lung metastasis that (based upon either biopsy or resection findings) was confirmed to be adenocarcinoma. Only one nodule recurred in the primary tumor lobe of a patient who had undergone segmentectomy; the remaining nine nodules recurred in a nonprimary tumor lobe and were clinically judged to more likely represent metastatic disease than metachronous primaries based on temporal evolution as documented on postoperative surveillance imaging studies.

Figure 4

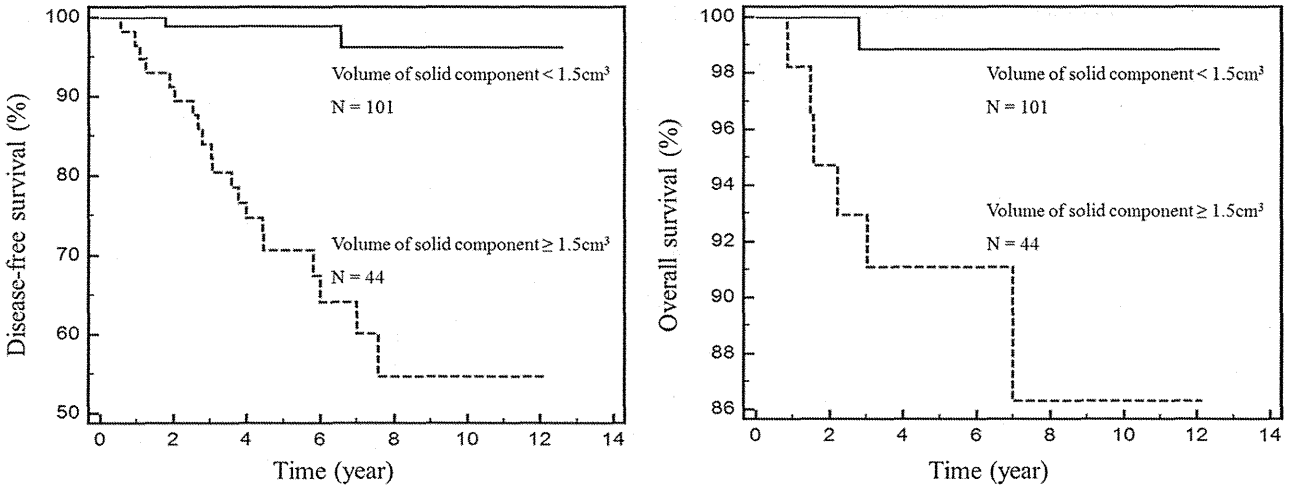

a. b.

Figure 4: Kaplan-Meier survival curves show that patients with solid tumor volume of 1.5 cm^3 or greater had a significantly lower probability of **(a)** disease-free ($P < .001$) and **(b)** overall survival ($P = .015$) than patients with solid tumor volume less than 1.5 cm^3.

Figure 5

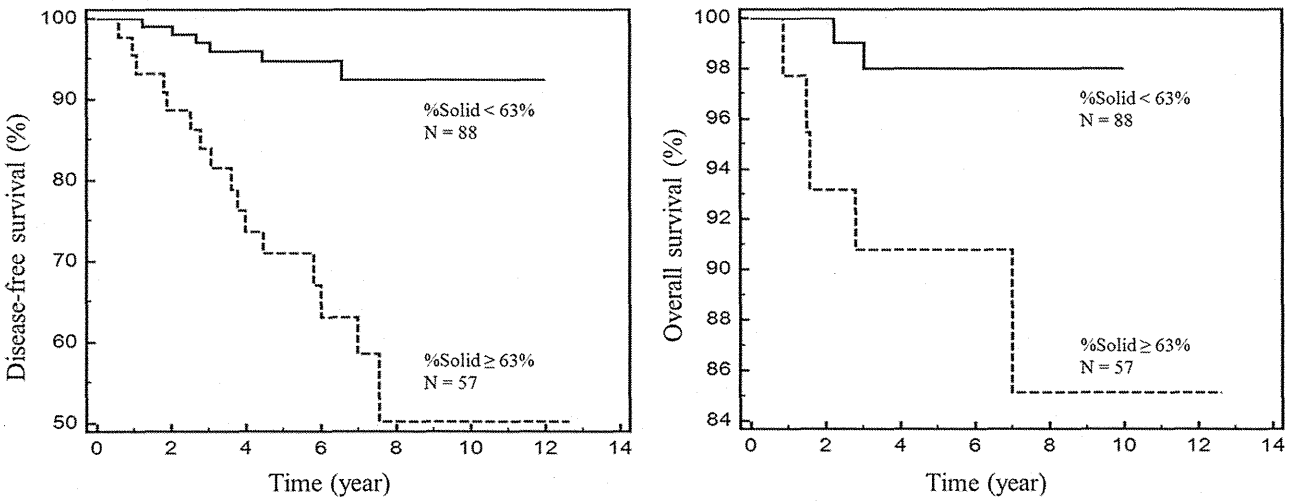

a. b.

Figure 5: Kaplan-Meier survival curves show that patients with percentage of solid tumor volume of 63% or greater had a significantly lower probability of **(a)** disease-free ($P < .001$) and **(b)** overall survival ($P = .010$) than patients with percentage of solid tumor volume of less than 63%.

Discussion

Clinical algorithms for optimal management of adenocarcinomas that manifest as subsolid nodules by using CT imaging remain an area of active controversy. In two guidelines recently published by the Fleischner Society (6) and American College of Chest Physicians (22), there was disagreement as to whether total diameter or diameter of only the solid component of a part-solid GGN should be used as the predictive feature that determines triage into alternate management pathways. A more fundamental controversy is whether solid tumor components visualized by using CT imaging should be measured on mediastinal or lung windows (23).

In our study, we used a volumetric automated computer-assisted method to analyze early-stage adenocarcinomas and link the analytic output, including volumetric measurements, to prognostic

Table 4

Quantitative Measurements in 22 Patients with Recurrence and Death

Case No.	Longest Diameter of Tumor (mm)	Longest Diameter of Solid Component (mm)	Solid Proportion (%)	Total Volume (cm^3)	Solid Volume (cm^3)	Percentage of Solid Volume (%)	Type of Surgery	Site of Recurrence
Recurrence								
1	13.7	4.8	35.04	1.26	0.48*	38.1†	Seg (LLL)	Lung (RUL)
2	19	16.7	87.89	2.88	2.04	70.8	L (LUL)	Lung (LLL)
3	21.4	18.1	84.58	4.5	2.87	63.8	Seg (LUL)	Lung (LUL)
4	10	10	100	0.45	0.34*	75.6	Seg (RLL)	Lung (multiple)
5	12	12	100	0.82	0.67*	81.7	L (RML)	Lung (RUL)
6	12	12	100	0.9	0.62*	68.9	Seg (LUL)	Lung (RML)
7	13.3	13.3	100	2.38	1.92	80.7	L (RUL)	Lung (LLL)
8	16	16	100	2.04	1.82	89.2	L (RUL)	Lymph node
9	18.5	14.5	78.38	2.44	1.8	73.8	L (LUL)	Bone
10	21	21	100	5.14	3.99	77.6	L (RML)	Lymph node
11	21.5	21.5	100	4.75	4.04	85.1	L (RLL)	Lung (LLL)
12	29.2	29.2	100	12.38	10.55	85.2	L (LLL)	Lymph node
13	18	18	100	3.35	2.92	87.2	L (RLL)	Lung (multiple)
14	19.1	19.1	100	3.28	2.78	84.8	Seg (LLL)	Lung (LUL)
15	22.1	22.1	100	6.53	4.93	75.5	L (RUL)	Lymph node
Death								
16	27.1	15	55.35	9.31	2.77	29.8†	Seg (RUL)	Pleura
17	15.3	10	65.36	0.74	0.48*	64.9	L (LUL)	Brain
18	12	12	100	0.87	0.64*	73.6	Seg (RLL)	Lymph node
19	15.1	15.1	100	4.46	4.01	89.9	L (LUL)	Lung (RUL)
20	18.3	18.3	100	1.95	1.53	78.5	Seg (LUL)	Lung (LUL)
21	19.9	19.9	100	4.09	3.18	77.8	L (RML)	Pleura
22	22.2	22.2	100	6.33	4.69	74.1	L (LLL)	Pleura

Note.—Information in parentheses is excision cite. L = lobectomy, Seg = segmentectomy, RUL = right upper lobe, RML = right middle lobe, RLL = right lower lobe, LUL = left upper lobe, LLL = left lower lobe.

* Volume of solid component was less than 1.5 cm^3.

† Percentage of solid volume was less than 63%.

factors and outcome measures. By using our custom software, automatic classification of nodules had excellent agreement with visual classification by radiologists; pure GGNs classified visually and by using software were associated with excellent prognosis with no recurrences or death observed. The uniformly excellent prognosis of pure GGNs after resection has been reported by several groups (24–26), and we are unaware of any cases of recurrence, even when nodules less than 3 cm of pure ground-glass composition are eventually found at pathologic examination to have invasive components (26).

Accurate segmentation of pulmonary nodules with or without ground-glass component is a challenging problem (27–31). In general, nodule segmentation is performed by using a combination of watershed and shape-analysis techniques; however, because these methods are edge-based, they cannot accurately delineate GGNs that typically share blurred margins with the surrounding lung parenchyma. Tan et al (31) have developed a probability-based method for segmentation of ground-glass nodules by using a Markov random model. By using this technique, the average overlap between computer and manual results for six nodules that contain ground-glass components was 60%. Kim et al (32) demonstrated that volumetric analysis was applicable for volume and mass measurement (12) of both pure and part-solid GGNs without measurement variation. In our study, we elected to segment nodules by using the mean FWHM of multiple density profile curves found by using CT imaging, drawn through the center of each tumor, with recognition that this would be an imperfect but reproducible technique that likely underestimates the extent of peripheral ground glass in some cases of part-solid GGNs. Incorporation of a three-dimensional line filter in our software also allowed for the elimination of both contiguous and intralesional vessels that may artificially increase the calculated total tumor or solid tumor volume measurements, respectively.

Similar to previous studies (4,33–35), we found that for stage I adenocarcinoma, measurement of total tumor was associated less with prognostic factors and outcome than it was with measurements of the solid component. In our study, percentage of solid volume of 63% or greater was associated

Figure 6

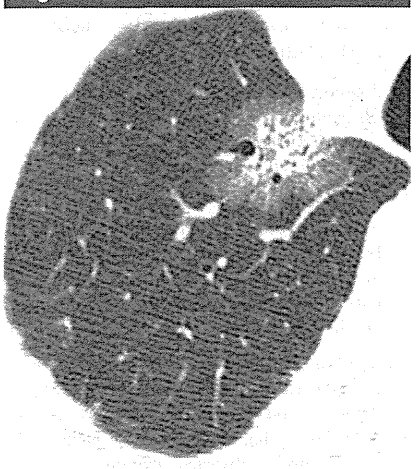

Figure 6: Thin-section CT image of a 27-mm nodule with multiple foci of solid components in a 65-year-old man who eventually died of recurrent disease. Volumetric measurements were total tumor volume, 9.31 cm^3; solid tumor volume, 2.77 cm^3; and percentage of solid tumor volume, 29.8%.

with the presence of pleural invasion; none of the four volumetric measurements were found to be associated with lymphatic or vascular invasion. This latter finding is discordant with results reported by Tsutani et al (33), who found that in 502 patients with clinical stage IA adenocarcinoma, solid tumor diameter was predictive of pleural, as well as of vascular and lymphatic invasion. Difference in results may be related to differences in the enrolled patient populations because our study included patients with pathologic stage I adenocarcinoma without lymph node metastases, and who therefore had a correspondingly lower prevalence of lymphatic invasion, vascular invasion, and pleural invasion compared with the population studied by Tsutani et al.

By using our volumetric automated computer-assisted analytic program, we found two volumetric measurements, solid volume of 1.5 cm^3 or greater and percentage of solid volume of 63% or greater, to be independent indicators associated with recurrence and/or death in patients with stage I adenocarcinoma. These results are consistent with those of previous studies that also reported that features found by using CT imaging, such as maximum diameter of the solid component (4,33) and ratio of maximum diameter of solid to ground-glass components exceeding 50% (2,36), can be associated with tumor recurrence after surgery. In our study, the two volumetric measurements were complementary, and used in combination they correctly identified 21 of 22 (95%) recurrent tumors. However, none of our evaluated two-dimensional measurements were found at multivariate analysis to be independent indicators associated with outcome; this lack of statistically significant results at multivariate analysis likely reflects the high degree of correlation between two-dimensional and volumetric variables and suggests that of the two quantitative sets, volumetric measurements may serve as better indicators associated with outcome. Compared with two-dimensional analysis that typically consists of tumor measurements on one or two images, volumetric analysis enables a more comprehensive and representative evaluation that may be particularly important for adenocarcinomas that have multiple foci of solid components.

Our study had several limitations. The study was retrospective in nature, and the relatively small number of enrolled patients may have resulted in inadequate statistical power to detect some CT features associated with prognosis. Results found in our study that had no statistically significant differences may have been caused by a true lack of differences or by the small sample size. Prospective studies with larger sample sizes will be needed to validate our results. Segmentation of subsolid nodules by using our custom software was imperfect with underestimation of the extent of peripheral ground glass. Given that ground glass is known to correspond to the lepidic noninvasive component of tumor, we chose not to perform manual edits so as to avoid the introduction of observer variability. Computer analysis of nodules was performed by only one operator who was required to select a tumor center point and draw an over-inclusive region of interest around the nodule before automated volumetric measurements could be performed. Ideally, the inclusion of one or more additional operators would have allowed for assessment of the reproducibility of the computer-generated volumetric measurements. Finally, inconsistency in the types of operations may have negatively affected outcomes in some patients who underwent sublobar resection; there are currently two ongoing randomized trials in Japan and North America to address whether segmentectomy can replace lobectomy as standard treatment (1).

In conclusion, our results demonstrated that two volumetric measurements (solid volume of ≥1.5 cm^3 and percentage of solid volume of ≥63%) are independent and complementary indicators associated with recurrence and/or death in patients with stage I adenocarcinoma. These results may have implications for determination of the optimal management of subsolid nodules.

Disclosures of Conflicts of Interest: M.Y. No relevant conflicts of interest to disclose. **Y.T.** No relevant conflicts of interest to disclose. **A.N.L.** No relevant conflicts of interest to disclose. **E.M.** No relevant conflicts of interest to disclose. **M.K.** No relevant conflicts of interest to disclose. **S.W.** No relevant conflicts of interest to disclose. **H.W.** No relevant conflicts of interest to disclose. **M.I.** No relevant conflicts of interest to disclose. **M.O.** No relevant conflicts of interest to disclose. **T.G.** No relevant conflicts of interest to disclose. **K.U.** No relevant conflicts of interest to disclose. **O.H.** No relevant conflicts of interest to disclose. **H.S.** No relevant conflicts of interest to disclose. **T.J.** No relevant conflicts of interest to disclose. **N.T.** No relevant conflicts of interest to disclose.

References

1. Travis WD, Brambilla E, Noguchi M, et al. International association for the study of lung cancer/american thoracic society/european respiratory society international multidisciplinary classification of lung adenocarcinoma. J Thorac Oncol 2011;6(2):244–285.

2. Ikehara M, Saito H, Yamada K, et al. Prognosis of small adenocarcinoma of the lung based on thin-section computed tomography and pathological preparations. J Comput Assist Tomogr 2008;32(3):426–431.

3. Nakazono T, Sakao Y, Yamaguchi K, Imai S, Kumazoe H, Kudo S. Subtypes of peripheral adenocarcinoma of the lung: dif-

ferentiation by thin-section CT. Eur Radiol 2005;15(8):1563–1568.

4. Sakao Y, Nakazono T, Tomimitsu S, et al. Lung adenocarcinoma can be subtyped according to tumor dimension by computed tomography mediastinal-window setting. Additional size criteria for clinical T1 adenocarcinoma. Eur J Cardiothorac Surg 2004;26(6):1211–1215.
5. Noguchi M. Stepwise progression of pulmonary adenocarcinoma—clinical and molecular implications. Cancer Metastasis Rev 2010;29(1):15–21.
6. Naidich DP, Bankier AA, MacMahon H, et al. Recommendations for the management of subsolid pulmonary nodules detected at CT: a statement from the Fleischner Society. Radiology 2013;266(1):304–317.
7. Yankelevitz DF, Reeves AP, Kostis WJ, Zhao B, Henschke CI. Small pulmonary nodules: volumetrically determined growth rates based on CT evaluation. Radiology 2000;217(1):251–256.
8. Ko JP, Rusinek H, Jacobs EL, et al. Small pulmonary nodules: volume measurement at chest CT—phantom study. Radiology 2003;228(3):864–870.
9. Das M, Mühlenbruch G, Katoh M, et al. Automated volumetry of solid pulmonary nodules in a phantom: accuracy across different CT scanner technologies. Invest Radiol 2007;42(5):297–302.
10. Marchianò A, Calabrò E, Civelli E, et al. Pulmonary nodules: volume repeatability at multidetector CT lung cancer screening. Radiology 2009;251(3):919–925.
11. Ko JP, Berman EJ, Kaur M, et al. Pulmonary Nodules: growth rate assessment in patients by using serial CT and three-dimensional volumetry. Radiology 2012;262(2):662–671.
12. de Hoop B, Gietema H, van de Vorst S, Murphy K, van Klaveren RJ, Prokop M. Pulmonary ground-glass nodules: increase in mass as an early indicator of growth. Radiology 2010;255(1):199–206.
13. Sato Y, Nakajima S, Shiraga N, et al. Three-dimensional multi-scale line filter for segmentation and visualization of curvilinear structures in medical images. Med Image Anal 1998;2(2):143–168.
14. Yanagawa M, Kuriyama K, Kunitomi Y, et al. One-dimensional quantitative evaluation of peripheral lung adenocarcinoma with or without ground-glass opacity on thin-section CT images using profile curves. Br J Radiol 2009;82(979):532–540.
15. Kuriyama K, Gamsu G, Stern RG, Cann CE, Herfkens RJ, Brundage BH. CT-determined pulmonary artery diameters in predicting pulmonary hypertension. Invest Radiol 1984;19(1):16–22.
16. Liu HL, Liu RR, Reeve DM, Shepard SJ, Willis CE. Measurement of CT radiation profile width using CR imaging plates. Med Phys 2005;32(9):2881–2887.
17. Pratt WK. Digital image processing. 4th ed. Los Altos, Calif: Wiley, 2007.
18. Yanagawa M, Tanaka Y, Kusumoto M, et al. Automated assessment of malignant degree of small peripheral adenocarcinomas using volumetric CT data: correlation with pathologic prognostic factors. Lung Cancer 2010;70(3):286–294.
19. Evangelou E, Kyzas PA, Trikalinos TA. Comparison of the diagnostic accuracy of lymphatic endothelium markers: Bayesian approach. Mod Pathol 2005;18(11):1490–1497.
20. Giatromanolaki A, Koukourakis MI, Theodossiou D, et al. Comparative evaluation of angiogenesis assessment with anti-factor-VIII and anti-CD31 immunostaining in non-small cell lung cancer. Clin Cancer Res 1997;3(12 Pt 1):2485–2492.
21. Maclure M, Willett WC. Misinterpretation and misuse of the kappa statistic. Am J Epidemiol 1987;126(2):161–169.
22. Gould MK, Donington J, Lynch WR, et al. Evaluation of individuals with pulmonary nodules: when is it lung cancer? Diagnosis and management of lung cancer, 3rd ed: American College of Chest Physicians evidence-based clinical practice guidelines. Chest 2013;143(5 Suppl):e93S–120S.
23. Arenas-Jiménez J. Measurement of solid component in part-solid lesions with a mediastinal window setting? Radiology 2013;268(1):305–306.
24. Nakamura H, Saji H, Ogata A, Saijo T, Okada S, Kato H. Lung cancer patients showing pure ground-glass opacity on computed tomography are good candidates for wedge resection. Lung Cancer 2004;44(1):61–68.
25. Park JH, Lee KS, Kim JH, et al. Malignant pure pulmonary ground-glass opacity nodules: prognostic implications. Korean J Radiol 2009;10(1):12–20.
26. Lim HJ, Ahn S, Lee KS, et al. Persistent pure ground-glass opacity lung nodules ≥ 10 mm in diameter at CT scan: histopathologic comparisons and prognostic implications. Chest 2013;144(4):1291–1299.
27. Revel MP, Lefort C, Bissery A, et al. Pulmonary nodules: preliminary experience with three-dimensional evaluation. Radiology 2004;231(2):459–466.
28. Zhao B, Reeves A, Yankelevitz D, Henshke C. Three-dimensional multi-criterion automatic segmentation of pulmonary nodules of helical computed tomography images. Opt Eng 1999;38(8):1340–1347.
29. Reeves AP, Chan AB, Yankelevitz DF, Henschke CI, Kressler B, Kostis WJ. On measuring the change in size of pulmonary nodules. IEEE Trans Med Imaging 2006;25(4):435–450.
30. Kauczor HU, Heitmann K, Heussel CP, Marwede D, Uthmann T, Thelen M. Automatic detection and quantification of ground-glass opacities on high-resolution CT using multiple neural networks: comparison with a density mask. AJR Am J Roentgenol 2000;175(5):1329–1334.
31. Tan Y, Schwartz LH, Zhao B. Segmentation of lung lesions on CT scans using watershed, active contours, and Markov random field. Med Phys 2013;40(4):043502.
32. Kim H, Park CM, Woo S, et al. Pure and part-solid pulmonary ground-glass nodules: measurement variability of volume and mass in nodules with a solid portion less than or equal to 5 mm. Radiology 2013;269(2):585–593.
33. Tsutani Y, Miyata Y, Nakayama H, et al. Prognostic significance of using solid versus whole tumor size on high-resolution computed tomography for predicting pathologic malignant grade of tumors in clinical stage IA lung adenocarcinoma: a multicenter study. J Thorac Cardiovasc Surg 2012;143(3):607–612.
34. Maeyashiki T, Suzuki K, Hattori A, Matsunaga T, Takamochi K, Oh S. The size of consolidation on thin-section computed tomography is a better predictor of survival than the maximum tumour dimension in resectable lung cancer. Eur J Cardiothorac Surg 2013;43(5):915–918.
35. Sakao Y, Miyamoto H, Sakuraba M, et al. Prognostic significance of a histologic subtype in small adenocarcinoma of the lung: the impact of nonbronchioloalveolar carcinoma components. Ann Thorac Surg 2007;83(1):209–214.
36. Hashizume T, Yamada K, Okamoto N, et al. Prognostic significance of thin-section CT scan findings in small-sized lung adenocarcinoma. Chest 2008;133(2):441–447.

Wilms' Tumor Gene *WT1* Promotes Homologous Recombination-Mediated DNA Damage Repair

Yusuke Oji,[1]*Naoya Tatsumi,[1] Junya Kobayashi,[2] Mari Fukuda,[3] Tazu Ueda,[3] Eri Nakano,[3] Chisae Saito,[3] Syohei Shibata,[3] Mihoko Sumikawa,[3] Hisashi Fukushima,[3] Akari Saito,[3] Nozomi Hojo,[3] Miyu Suzuki,[3] Tomoko Hoshikawa,[3] Tsutomu Shimura,[4] Eiichi Morii,[5] Yoshihiro Oka,[6] Naoki Hosen,[1] Kenshi Komatsu,[2] and Haruo Sugiyama[3]

[1]*Department of Cancer Stem Cell Biology, Osaka University Graduate School of Medicine, Osaka, Japan*
[2]*Radiation Biology Center, Kyoto University, Kyoto, Japan*
[3]*Department of Functional Diagnostic Science, Osaka University Graduate School of Medicine, Osaka, Japan*
[4]*Department of Environmental Health, National Institute of Public Health, Saitama, Japan*
[5]*Department of Pathology, Osaka University Graduate School of Medicine, Suita, Osaka, Japan*
[6]*Department of Cancer Immunology, Osaka University Graduate School of Medicine, Osaka, Japan*

The Wilms' tumor gene *WT1* is overexpressed in leukemia and various types of solid tumors and plays an oncogenic role in these malignancies. Alternative splicing at two sites yields four major isoforms, 17AA(+)KTS(+), 17AA(+)KTS(−), 17AA(−)KTS(+), and 17AA(−)KTS(−), and all the isoforms are expressed in the malignancies. However, among the four isoforms, function of WT1[17AA(−)KTS(+)] isoform still remains undetermined. In the present study, we showed that forced expression of WT1[17AA(−)KTS(+)] isoform significantly inhibited apoptosis by DNA-damaging agents such as Doxorubicin, Mitomycin, Camptothesisn, and Bleomycin in immortalized fibroblast MRC5SV and cervical cancer HeLa cells. Knockdown of Rad51, an essential factor for homologous recombination (HR)-mediated DNA repair canceled the resistance to Doxorubicin induced by WT1[17AA(−)KTS(+)] isoform. GFP recombination assay showed that WT1 [17AA(−)KTS(+)] isoform alone promoted HR, but that three other WT1 isoforms did not. WT1[17AA(−)KTS(+)] isoform significantly upregulated the expression of HR genes, *XRCC2*, *Rad51D*, and *Rad54*. Knockdown of *XRCC2*, *Rad51D*, and *Rad54* inhibited the HR activity and canceled resistance to Doxorubicin in MRC5SV cells with forced expression of WT1[17AA(−)KTS(+)] isoform. Furthermore, chromatin immunoprecipitation (ChIP) assay showed the binding of WT1[17AA(−)KTS(+)] isoform protein to promoters of *XRCC2* and *Rad51D*. Immunohistochemical study showed that Rad54 and XRCC2 proteins were highly expressed in the majority of non-small-cell lung cancer (NSCLC) and gastric cancer, and that expression of these two proteins was significantly correlated with that of WT1 protein in NSCLCs. Our results presented here showed that WT1[17AA(−)KTS(+)] isoform had a function to promote HR-mediated DNA repair.

Key words: WT1; homologous recombination; chemoresistance; DNA repair; HR factors

INTRODUCTION

Malignant tumors are one of the leading causes of death and a major public health problem in developed countries. Despite recent advances in diagnostic tools and therapeutic modalities, prognosis still remains unsatisfactory for patients with advanced diseases, and even in early-stage patients, recurrence occurs after chemotherapy in a significant portion. Resistance of tumor cells to chemotherapeutic drugs, chemoresistance is the primary cause of failure in chemotherapeutic treatment for most tumors and is induced by multiple mechanisms, including abnormal membrane receptor transport, enhanced inactivation of drug metabolite, in particular, increased DNA damage repair, and alterations in the apoptosis pathways. Since functions of many chemotherapeutic agents are primarily induction of cell death through DNA damage, it is important to understand the mechanisms by which tumor cells acquire resistance to DNA damage for overcoming chemoresistance [1].

The *WT1* gene encodes a protein with four zinc fingers and is alternatively spliced at two sites (17AA site in exon 5 and KTS site in exon 9), which yields four major isoforms 17AA(−)/KTS(−) (WTA), 17AA-(+)/KTS(−) (WTB), 17AA(−)/KTS(+) (WTC), and 17AA(+)/KTS(+) (WTD). WT1(KTS−) isoforms have been well characterized as a transcriptional factor that is involved in transcriptional regulation of many genes, for example, such as PDGF-A chain [2], IGF-II [3], IGF-IR [4], Amphiregulin [5], and SRPK1 [6]. While WT1 (KTS+) isoform have been implicated in mRNA metabolism including regulation of splicing

Conflict of intrest: The authors declare no conflicts of interest.

*Correspondence to: Department of Cancer Stem Cell Biology, Osaka University Graduate School of Medicine, 1-7 Yamada-oka, Suita, Osaka 565-0871, Japan.

Received 14 May 2014; Revised 5 October 2014; Accepted 10 October 2014

DOI 10.1002/mc.22248

Published online in Wiley Online Library (wileyonlinelibrary.com).

based on the findings that WT1(KTS+) protein was associated with splicing factors in the nucleus [7] and that WT1(KTS+) protein directly bound to IGF-2 exon 2 RNA and the normal subnuclear localization of WT1 protein was RNase, but not DNase, sensitive [8].

The *WT1* gene was originally isolated as a tumor suppressor gene responsible for Wilms' tumor, a neoplasm of the childhood [9]. However, many research groups are nowadays convinced that the *WT1* gene plays an oncogenic role rather than a tumor suppressor based on the following findings: (a) the wild-type *WT1* gene is overexpressed in human leukemia [10] and a wide variety of solid tumors such as lung [11], colon [12], breast [13,14], gastric [15], head and neck [16] and pancreatic cancer [17], astrocytic tumors [18], bone and soft-tissue sarcoma [19], and melanoma [16,20] and higher expression levels of WT1 mRNA correlated with poor prognosis in leukemia [10], breast cancer [14], and soft-tissue sarcoma [21]; (b) growth of WT1-expressing leukemia and solid tumor cells was inhibited by suppression of WT1 expression [18,22,23]; (c) proliferation of 32D cl3 myeloid progenitor [24] and normal myeloid cells [25] with differentiation block was induced by constitutive expression of WTD isoform in response to granulocyte colony-stimulating factor (G-CSF); and (d) WTA isoform induced cytoskeletal changes and promoted in vitro invasion through modulation of expression of actin binding proteins [26], and WTB and WTD isoforms stabilized the mitochondrial membrane potential and inhibited apoptosis induced by DNA damaging agents such as doxorubicin and etoposide in leukemia [27] and solid tumor cells [28]. Furthermore, WT1 that could directly be transactivated by HIF-1 [29] supports tumor formation through promotion of angiogenesis by transcriptional upregulation of VEGF [30] and enhancement of proliferation and migration of endothelial cells [31]. Moreover, WTB isoform could render tumor cells escape from immunosurveillance by transcriptional upregulation of CD95L in T-leukemic cells [32]. All of the four WT1 isoforms were expressed in leukemia [27,33] and solid tumors, including lung cancer [11] and sarcoma [19], which allowed us to assume orchestrated oncogenic functions of these four WT1 isoforms. However, among the four WT1 isoforms, the precise function of WTC isoform still remains undetermined.

In the present study, we demonstrate for the first time that among the four WT1 isoforms, WTC isoform alone promotes homologous recombination (HR)-mediated DNA damage repair through upregulation of HR genes such as XRCC2, Rad51D, and Rad54.

MATERIALS AND METHODS

Cells and Cell Culture

MRC5SV-pDRGFP and HeLa-pDRGFP cells were cultured in DMEM supplemented with 10% FBS containing 1 μg/mL of puromycin [34,35]. At the initiation of the present study, the cell lines were authenticated by STR analysis. MRC5SV pDR-GFP cells (WTA-MRC, WTB-MRC, WTC-MRC, WTD-MRC, and Mock-MRC) with forced expression of one each of four WT1 isoforms (WTA, WTB, WTC, and WTD) or empty vector pcDNA3.1+ (Invitrogen, Carlsbad, CA) were established. HeLa-pDR-GFP cells (WTC-HeLa and Mock-HeLa) with forced expression of WTC isoform or empty vector pcDNA3.1+ were also established. These cells were cultured in Dulbecco's modified essential medium (DMEM) supplemented with 10% fetal bovine serum (FBS) containing 1 μg/mL of puromycin and 700 μg/mL of G418.

Reagents

Doxorubicin (DOX), Camptothesin (CPT), and Bleomycin (BLEO) were purchased from Sigma-Aldrich (St Louis, MO). Mitomycin (MMC) were purchased from Nacalai Tesque (Kyoto, Japan).

Tissue Samples

Tumor tissues were obtained with informed consent at Osaka University Hospital from 44 non-small cell lung cancer and 15 gastric cancer patients. For double-stain immunohistochemistry of non-small cell lung cancer, tissue microarray was purchased from Super Bio Chips (Seoul, Korea).

siRNA and Transfection

siRNA targeting Rad51, XRCC2, and Rad51D (siRad51, siXRCC2, and siRad51D, respectively) (Santa Cruz Biotechnology, Santa Cruz, CA) and control siRNA targeting Luciferase (siLuc) (Doujindo laboratories, Kumamoto, Japan) were used for knockdown of these genes. siRNA (2 μg) was transfected into 1×10^5 cells using lipofectamine 2000 (Invitrogen) according to the manufacturer's instructions.

Western Blot Analysis

Proteins were separated by SDS-PAGE and transferred to Immobilon polyvinylidene difluoride membrane (Millipore Corp., Bedford, MA). After blocking of non-specific binding, the membranes were incubated with a first antibody, followed by incubation with the corresponding second antibody conjugated with alkaline phosphatase, and visualized using BCIP/NBT kit (Nacalai Tesque). WT1 antibody (6F-H2) was purchased from Dako Cytometry (Glostrup, Denmark). Antibodies for Rad51 (sc-53428), XRCC2 (N-20, sc-5895), Rad51D (C-16, sc-33090), Rad54 (sc5849), and Rad52 (sc8350) were purchased from Santa Cruz Biotechnology. Antibody for GAPDH (MAB374) was purchased from Millipore Corp. and antibodies for FEN1 and Mus81 were purchased from Abcam (Cambridge, UK). They were used as primary antibodies.

Analysis of Apoptosis by Flowcytometry

To assess apoptotic cells, 1×10^5 cells were washed with PBS, and stained with Annexin V- fluorescein

isothiocyanate (FITC) and propidium iodide (PI) at room temperature for 15 min in the dark using MEBCYTO Apoptosis Kit (Medical and Biological Laboratories Co., Ltd, Aichi, Japan) according to the manufacturer's instructions. Then, the stained cells were analyzed by FACSort flowcytometer (Becton Dickinson, San Jose, CA). Frequencies (%) of Annexin V-positive apoptotic cells were shown as those of Annexin V-positivie cells to the total cells examined.

Analysis of Cell Cycle Distribution by Flowcytometry

To assess cell cycle distribution, 1×10^5 cells were harvested, washed once with PBS, resuspended in 100 μL of ice-cooled PBS followed by adding 1 mL of ice-cooled 80% ethanol with pipetting, and fixed at −20°C overnight. After incubation at room temperature for 10 min, cells were resuspended in 400 μL of PBS containing 5 μg/mL of propidium iodide (PI, Nacalai Tesque, Kyoto, Japan) and 200 μg/mL of RNase A (Nacalai Tesque) and incubated at 37°C for 30 min in the dark. Flowcytometry was performed on a FACS Calibur (Beckton Dickinson), and cell cycle distribution was analyzed using Mod Fit ver.2 software (Verity Software Home, Topsham, ME).

Immunofluorescence Study

Cells were placed onto glass slides by cytospin. After fixation with 4% paraformaldehyde in PBS for 15 min on ice, the cells were twice treated with 1% Triton-X in PBS for 5 min, followed by treatment with methanol for 10 min. After blocking with PBS containing 0.5% BSA for 30 min, the cells were stained with anti-Ser-139-phosphorylated H2AX (γH2AX) antibody (2F3, Biolegend 613402) at 1:100 dilution overnight, followed by Alexa Fluor 488-conjugated secondary antibody (Life Technologies, Carlsbad, CA) at 1:500 dilution for 2 h. The cells were washed, counterstained with 4V, 6V diamidino-2-phenylindole (DAPI), and mounted with Prolong anti-fade reagent (Life Technologies). The number of nuclei containing more than five γH2AX foci in more than 400 nuclei was counted using fluorescence microscopy BZX-700 (Keyence, Osaka, Japan).

GFP Recombination Assay

HR frequency was measured by using pDR-GFP vector as a substrate of HR [35]. pDR-GFP vector was composed of two differentially mutated GFP genes oriented as direct repeats. The upstream GFP was mutated to contain the recognition site for I-Sce I restriction enzyme and two in-frame stop codons, which terminated translation and inactivated the protein (SceGFP). Downstream sequence of the SceGFP was a 5′ and 3′-truncated GFP gene, internal GFP (iGFP). Homologous sequences in the two mutated GFP genes were separated by 3.7 kb. pCBAS vector encoding restriction enzyme I-Sce I (10 μg) was introduced into MRC5 SV and HeLa cells transduced with pDR-GFP vector (MRC5 SV pDR-GFP and HeLa pDR-GFP cells) (6×10^5 cells) by electroporation at 220 V and 650 μFD to generate DNA DSB at the I-Sce I restriction site within SceGFP sequence. After 72 h of culture, GFP expression in these cells, which indicated the HR-mediated DNA repair at the I-SceI site from the iGFP gene on the same chromatid or sister chromatid, was analysed by flowcytometry.

Real-Time RT-PCR

Total RNA was isolated using Trizol (Invitrogen) and reverse transcribed using murine Moloney leukemia virus (M-MLV) reverse transcriptase (Promega, Madison, WI) accoding to the manufacturer's instructions. To measure the mRNA expression levels of HR genes, real-time PCR was performed for 40 cycles (95°C for 10 s and annealing temperature (60°C for Rad51, Rad51B, Rad51C, XRCC2, XRCC3, and Rad54, 58°C for BRCA2 and GAPDH, and 62°C for Rad51D and BRCA1) for 30 s) using GoTaq qPCR Master Mix (Promega) on Chrome 4 system (Bio-Rad Laboratories, Hercules, CA). Sequences of primer pairs were as follows. Rad51 forward primer: 5′-tga gct ttc agc cag gca ga-3′, Rad51 reverse primer: 5′-cca ctt gag cta cca cct ga-3′, Rad51B forward primer: 5′-cgg ctt atg gga taa aag ca-3′, Rad51B reverse primer: 5′-ctt cgt cca aag cag aaa gg-3′, Rad51C forward primer: 5′-gca tac cca ggg ctt cat aa-3′, Rad51C reverse primer: 5′-aaa ctg ctt cac ctg cca ct-3′, Rad51D forward primer: 5′-aag gga ggg tat gac ctg ct-3′, Rad51D reverse primer: 5′-ggt aca gct ggc agg aag ag-3′, BRCA1 forward primer: 5′-ctg ctt gaa gtc tcc ctt gg-3′, BRCA1 reverse primer: 5′-act ctg tgc ttc cag ccc ta-3′, BRCA2 forward primer: 5′-agc tct tca ccc tgc aaa aa-3′, BRCA2 reverse primer: 5′-cca atg cct cgt aac aac ct-3′, XRCC2 forward primer: 5′-acc cag gca gta cca ttc ag -3′, XRCC2 reverse primer: 5′-gtt cat gtc ctt tgc cca ct-3′, XRCC3 forward primer: 5′-act gtg ccc cac aaa act tc-3′, XRCC3 reverse primer: 5′-gac cct cct tcc tct caa cc-3′, Rad54 forward primer: 5′-gaa gcg agc caa ggt tgt ag-3′, Rad54 reverse primer: 5′-cca tgg ctt gtt cat cat tg-3′, GAPDH forward primer: 5′-gcc aaa agg gtc atc atc tc-3′, and GAPDH reverse primer: 5′-gta gag gca ggg atg atg ttc-3′. Distilled water was used as a negative control for every PCR run. Verification of real-time RT-PCR amplicons was performed using melting curve analysis. Expression levels of the individual genes in K562 leukemia cells were defined as 1.0. To normalize the difference in RNA loading for RT-PCR in individual samples, the expression levels of the genes divided by those of GAPDH gene were defined as relative expression levels of the genes.

Chromatin Immunoprecipitation (ChIP) Assay

MRC5SV cells with forced expression of WTC isoform (WTC-MRC cells) (2×10^6 cells) were treated with 1% formaldehyde in 1 mL of medium for 5 min at room temperature to cross-link DNA binding proteins to genome DNA and cross-linking was stopped by the addition of 100 μL of 1.5 M glycine. After wash with PBS containing 2% FBS, the cells were

resuspended in 200 μL of SDS lysis buffer [50 mM Tris-HCl pH8.0, 10 mM EDTA pH8.0, 1% SDS, 1 mM PMSF, 1 μM aprotinin]. The cell suspension was 15 times sonicated on ice for 15 s each at output and duty parameters of 2 and continuous, respectively, with a UD-201 ultrasonic disruptor (TOMY, Tokyo, Japan) to produce genome DNA fragments with an average length of 200–600 bp. After centrifugation, the supernatant was transferred to a new tube, diluted with 1.8 mL of ice-cold ChIP dilution buffer (50 mM Tris-HCl pH8.0, 167 mM NaCl, 1.1% TritonX-100, 0.11% sodium deoxycholate, 1 mM PMSF, 1 μM aprotinin), and precleared with protein G-agarose beads at 4°C for 2 h. After removal of beads by brief centrifugation, the chromatin solution was divided into three new tubes and immunoprecipitated with 3 μg of each of protein G-agarose beads-bound anti-WT1 C-19 antibody (Santa Cruz Biotechnology), anti-acetylated Histone3 antibody (AcH3 Ab, Upstate, #06–599), non-immune rabbit IgG (Dako) at 4°C overnight. The immune complex was eluted with 100 μL of elution buffer (10 mM Tris-HCl pH8.0, 300 mM NaCl, 5 mM EDTA pH8.0, 0.5% SDS), and formaldehyde cross-linking was reversed by heating at 65°C for 4 h. Genomic DNA was purified, resolved in 20 μL of distilled water and analyzed by quantitative real-time PCR. Real-time PCR was performed for 40 cycles (95°C for 10 s and annealing temperature 60°C for 30 s) using GoTaq qPCR Master Mix (Promega, Madison, WI) on Chrome 4 system (Bio-Rad Laboratories, Hercules, CA). Fold enrichment relative to non-immune IgG was calculated for WT1- and AcH3-immunoprecipitated samples by delta Ct method: Fold enrichment= 2^[(Ct-IgG) – (Ct-WT1) or (Ct-AcH3)]. The PCR primers were as follows. XRCC2-promoter X1-X2 forward primer: 5′-atg ctg gca ccc tct gcc ac-3′, XRCC2-promoter X1-X2 reverse primer: 5′-gag gag aga cct cgt atg tta t-3′, Rad51D-promoter R1 forward primer: 5′-gat ctc aaa atg cct gac acc t-3′, Rad51D-promoter R1 reverse primer: 5′-gcc tta gct tct acg gac aaa g-3′, Rad51D-promoter R2 forward primer: 5′-cac aca tga tct ctg ctc tca g-3′, Rad51D-promoter R2 reverse primer: 5′- gaa act gag gtt cag tga ggt t-3′, Rad51D-promoter R3 forward primer: 5′-gtg tgt gtt cta tat aac caa gg-3′, Rad51D-promoter R3 reverse primer: 5′-cac aca ggt ctc gaa cta ctg-3′, Rad51D-promoter R4 forward primer: 5′-cag tag ttc gag acc tgt gtg-3′, Rad51D-promoter R4 reverse primer: 5′- gtg aga tct cag ctt tgc agc-3′, Rad51D-promoter R5 forward primer: 5′-gcc tgt gtc ctc tct agg aag-3′, and Rad51D-promoter R5 reverse primer: 5′-cct gag aag ctg gat cat ctc-3′.

Immunohistochemistry

Formalin-fixed tissue sections were cut from each paraffin-block. After dewaxing and rehydration, the sections were antigen retrieved using Target Retrieval solution (pH9.0) (Dako Cytometry) and reacted with the first antibody at 1:100 dilution at 4°C overnight and then reacted with Dako Envision kit/HRP (Dako Cytometry) at room temperature for 30 min. After treatment with 3% H_2O_2 solution to reduce endogenous peroxidase activity, immunoreactive WT1, XRCC2, and Rad54 proteins were visualized using Diaminobenzidine (DAB). The sections were then counterstained with hematoxyline. The intensity of stain in tumor cells was scored as positive (increased staining in tumor cells compared to that in normal cells) or negative (less or negative staining in tumor cells) by a pathologist. Rad54 antibody (ab10705) and XRCC2 antibody were purchased from Abcam and Millipore, respectively. Non-immune rabbit immunoglobulin (Dako Cytometry) was used as negative control for nonspecific staining.

Double staining of WT1 and one each of Rad54, XRCC2, and Rad51 was performed by the method of Lan et al. [36] with modifications. After antigen retrieval described above, the sections were reacted with one each of Rad54 (ab10705, Abcam, at 1:200 dilution), XRCC2 (ab58466, Abcam, at 1:200 dilution), and Rad51 (ab88572, Abcam, at 1:165 dilution) antibodies at 4°C overnight and then reacted with Dako Envision kit/HRP (Dako Cytometry) at room temperature for 30 min. Rad54, XRCC2, and Rad51 proteins were visualized in brown color using Diaminobenzidine (DAB). Next, to block crossreactivity to Rad54, XRCC2, and Rad51 antibody, the sections were incubated in Target Retrieval solution (pH9.0) (Dako Cytometry) at 98°C for 10 min. After wash with water and 0.1% Tween-20 in PBS, the sections were reacted with anti-WT1 6F-H2 antibody at 1:100 dilution at 4°C overnight and then reacted with EnVision G/2 System A/P, Rabbit/Mouse (Permanent Red) (Dako Cytometry). After treatment with 3% H_2O_2 solution to reduce endogenous peroxidase activity, WT1 protein was visualized in red color. The sections were then counterstained with hematoxyline.

Statistical Analysis

The statistical significance in a difference between arithmetical means of test groups was assessed by unpaired *t* or Kruskal–Wallis test. After Kruskal–Wallis test, Scheffe's *F* test was used as a post hoc test. Correlation between HR gene protein and WT1 protein expression in tumor cells was analyzed by using Spearman's rank correlation coefficient test.

RESULTS

WTC Isoform Inhibits DNA-Damaging Agent-Induced Apoptosis

Each of the four WT1 isoforms is considered to have different functions. The functions of three WT1 isoforms (WTA, WTB, and WTD) other than WTC isoform had been reported so far, but precise function of WTC isoform remained undetermined. To examine whether or not WTC isoform induced resistance to

chemotherapeutic agents, WT1-non-expressing MRC5 SV pDR-GFP fibroblastic cells (MRC cells), in which homologous recombination (HR)-mediated DNA repair was detectable as a GFP expression, were stably transduced with WTC isoform (WTC-MRC) or control vector pcDNA3.1(+) (Mock-MRC), treated with one each of four DNA-damaging agents, DOX, CPT, MMC, and Bleo for 24 h, and analysed for apoptosis. Flowcytometric analysis showed that DOX-, CPT-, MMC-, and Bleo-induced apoptosis was significantly inhibited by 39.6, 38.0, 34.9, and 37.1%, respectively, in WTC-MRC cells, compared to Mock-MRC cells (Figure 1A).

To confirm this phenomenon, HeLa cells were stably transduced with WTC isoform (WTC-HeLa) or control vector pcDNA3.1+ (Mock-HeLa), treated with one each of the three DNA-damaging agents, DOX, CPT, and MMC for 24 h, and analysed for apoptosis. Flowcytometric analysis showed similar results that DOX-, CPT-, and MMC-induced apoptosis was significantly inhibited by 53.6, 36.8, and 45.3%, respectively, in WTC-HeLa cells, compared to Mock-HeLa cells (Figure 1B). These results indicated that WTC isoform inhibited DNA-damaging agent-induced apoptosis.

To examine the possibility that resistance to DNA-damaging agents induced by forced expression of WTC isoform was by the cell cycle regulation, cell cycle distribution of WTC-MRC and Mock-MRC cells was examined (Figure 1C). Flowcytometric analysis showed that frequency of cells in S phase, which is the target for most of DNA-damaging agents, slightly decreased in WTC-MRC cells compared to Mock-MRC cells, although it was not statistically significant ($P = 0.06$). Frequency of cells in G2/M phase significantly increased in WTC-MRC cells compared to Mock-MRC cells.

WTC Isoform Promotes Homologous Recombination-Mediated DNA Damage Repair

One of the important mechanisms by which cancer cells acquire the resistance to DNA-damaging chemotherapeutic agents is homologous recombination (HR) that repairs DNA double strand break. Therefore,

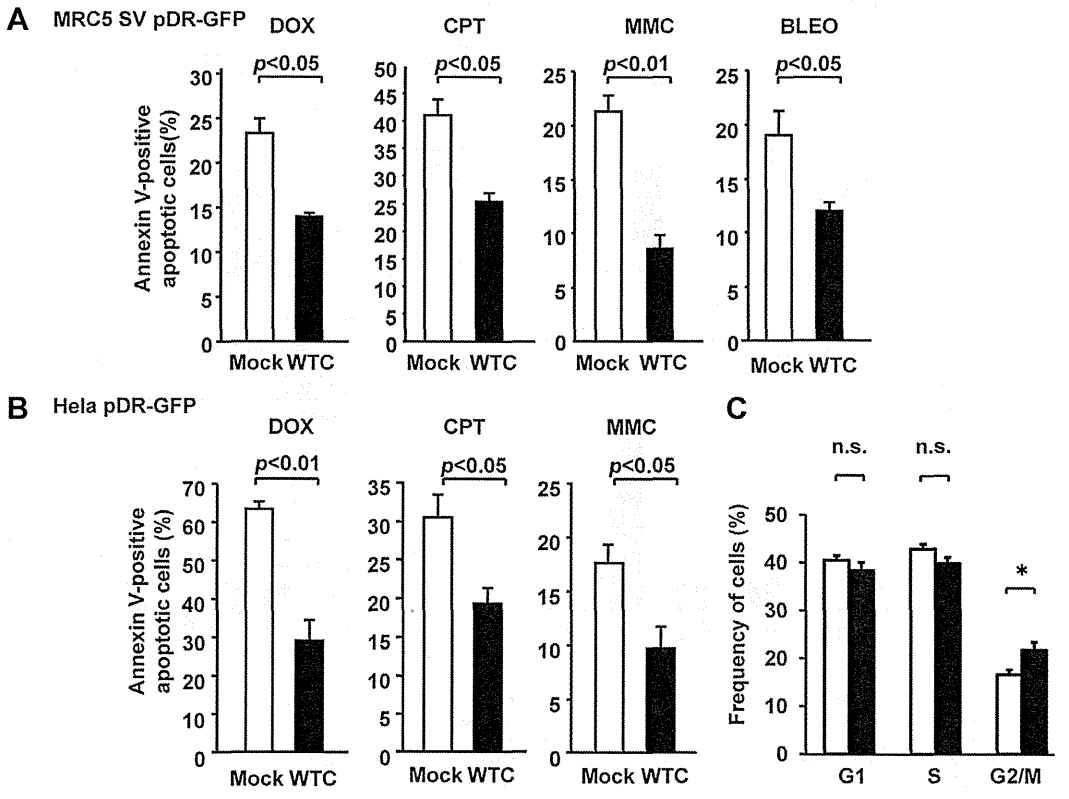

Figure 1. WTC isoform inhibits DNA-damaging agent-induced apoptosis. WTC-MRC and Mock-MRC (A), or WTC-HeLa and Mock-HeLa (B) cells were treated with DOX (2 μM), CPT (10 μM), MMC (2 μg/mL), or BLEO (10 μg/mL) for 24 h and analysed for apoptosis by flowcytometry. Columns, means of frequencies (%) of Annexin V-positive apoptotic cells; Bars, SE. Results were obtained from three independent experiments using three different cell clones. (C) Cell cycle distribution of cells. Open and closed columns represent means of frequencies of cells in the indicated phase of the cell cycle of Mock-MRC and WTC-MRC cells, respectively. Bars, SE. Results were obtained using three different cell clones for each test group.

whether or not the resistance to DNA-damaging chemotherapeutic agents induced by WTC isoform was involved in HR-mediated DNA repair was examined. siRNA that targeted an essential HR factor Rad51 or control siRNA was transfected into WTC-MRC and WTC-HeLa cells (Figure 2A), and then, these cells were treated with DOX for 24 h and analysed for apoptosis. Flowcytometric analysis showed that knockdown of Rad51 significantly canceled the resistance to DOX in both WTC-MRC and WTC-HeLa cells (Figure 2A). These results indicated that WTC isoform suppressed DNA-damaging agents-induced apoptosis through HR-mediated DNA damage repair.

To confirm that WTC promoted HR, pDR-GFP HR reporter assay, in which HR-mediated DNA repair of DNA double strand break (DSB) was detectable as induction of GFP expression, was performed (Figure 2B). MRC cells transduced with WTA, WTB, WTC, WTD, or mock (Figure 2C) were transduced with pCBAS vector coding restriction enzyme I-Sce I to induce DNA DSB and cultured for 72 h, and then HR-mediated expression of GFP was analysed by flowcytometry. The frequency of GFP-positive cells was significantly higher in WTC-MRC cells compared to WTA-, WTB-, WTD-, and Mock-MRC cells (Figure 2B).

To examine the possibility that forced expression of WTC induced DNA damages and as a result increased activity of HR-mediated DNA damage repair in MRC cells, frequency of γH2AX foci-positive cells was analyzed in WTA-, WTB-, WTC-, WTD-, and Mock-MRC cells. Immunofluorescence studies showed that no significant difference was observed in frequency of γH2AX foci-positive cells among these cells (Figure 2D).

These results indicated that WTC isoform alone promoted DNA DSB repair through promotion of HR.

WTC Isoform Upregulates Homologous Recombination Genes

To examine the mechanism by which WTC isoform promotes HR, expression of HR genes, such as Rad51, Rad51B, Rad51C, Rad51D, XRCC2, XRCC3, BRCA1, and BRCA2, which were involved in early steps of HR,

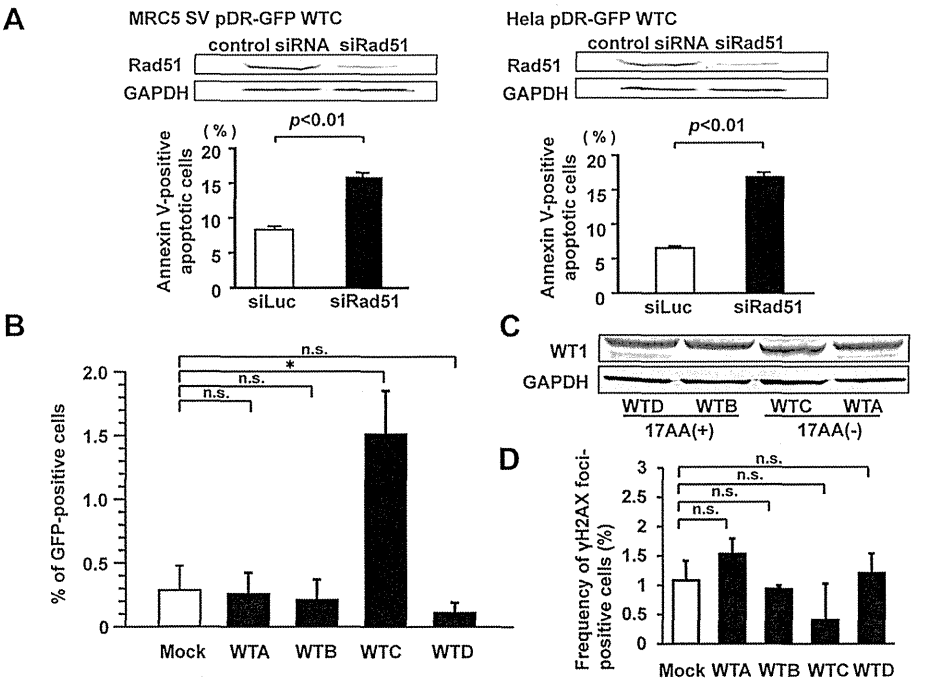

Figure 2. WTC isoform promotes HR-mediated DNA damage repair. (A) Cells were transfected with siRNA targeting Rad51 (siRad51) or control siRNA (siLuc) and then treated with DOX at the concentrations of 2 μM for 24 h. Upper, Western blot showing knockdown of Rad51 protein by siRad51. Lower, Frequencies (%) of Annexin V-positive apoptotic cells detected by flowcytometry. Columns, Means of frequencies of Annexin V-positive apoptotic cells. Bars indicate SE. (B) Increase in frequencies of HR by forced expression of WTC isoform. pCBAS vector was introduced by electroporation into MRC-pDR-GFP cells with forced expression of one each of WT1 isoforms or a mock gene to generate DNA DSB. HR-mediated GFP expression was analysed by flowcytometry after 72 h of culture. Column, Means of GFP- positive cells. Bars indicate SE. closed squares, WT1 isoform-transduced cells; open squares, control pcDNA 3.1+ vector-transduced cells. Results were obtained from three independent experiments using three different cell clones. (C) Representative results of Western blot analysis showing the expression of respective WT1 isoform protein. (D) Frequency of γH2AX foci-positive cells determined by immunofluorescence study. The number of nuclei containing more than five γH2AX foci in more than 400 nuclei was counted. (B–D) WTA, WTB, WTC, WTD, and Mock indicate WTA-, WTB-, WTC-, WTD-, and Mock-MRC cells, respectively.

was examined by real-time RT-PCR in WTC-MRC and Mock-MRC cells (Figure 3). Among the eight HR-related genes, XRCC2 and Rad51D were significantly higher in WTC-MRC cells at both mRNA and protein expression levels, compared to Mock-MRC cells (Figure 3A and B). It is known that XRCC2 and Rad51D form a heterodimer and could play an important role in loading of Rad51 onto single strand DNA at the sites of DNA damage [37]. Therefore, the role of XRCC2 and Rad51D in WTC isoform-induced promotion of HR was examined. WTC-MRC cells were transfected with the both of siRNAs targeting XRCC2 and Rad51D, and then pCBAS vector was transduced into the cells two days later. Flowcytometric analysis showed that HR-mediated expression of GFP was significantly suppressed by simultaneous knockdown of XRCC2 and Rad51D (Figure 3C and D). To confirm the involvement of XRCC2 and Rad51D in resistance to DOX induced by WTC, WTC-MRC cells were treated with DOX for 24 h two days after the transfection with both of the siRNAs targeting XRCC2 and Rad51D. Knockdown of both XRCC2 and Rad51D significantly canceled the resistance to DOX in WTC-MRC cells (Figure 3D).

Next, to determine the effect of WTC on mid to late processes of HR, expression of HR genes, such as Rad52, Rad54, FEN1, and Mus81, which were involved in mid to late processes of HR, was examined by Western blot in WTC-MRC and Mock-MRC cells. Among these four HR proteins, Rad54 protein was highly expressed in WTC-MRC cells compared to Mock-MRC cells (Figure 4A). However, significant difference in mRNA expression levels of Rad54 was not observed between WTC- and Mock-MRC cells (Figure 4B).

To confirm the role of Rad54 in WTC isoform-induced promotion of HR, WTC-MRC cells were transfected with siRNA targeting Rad54, and then

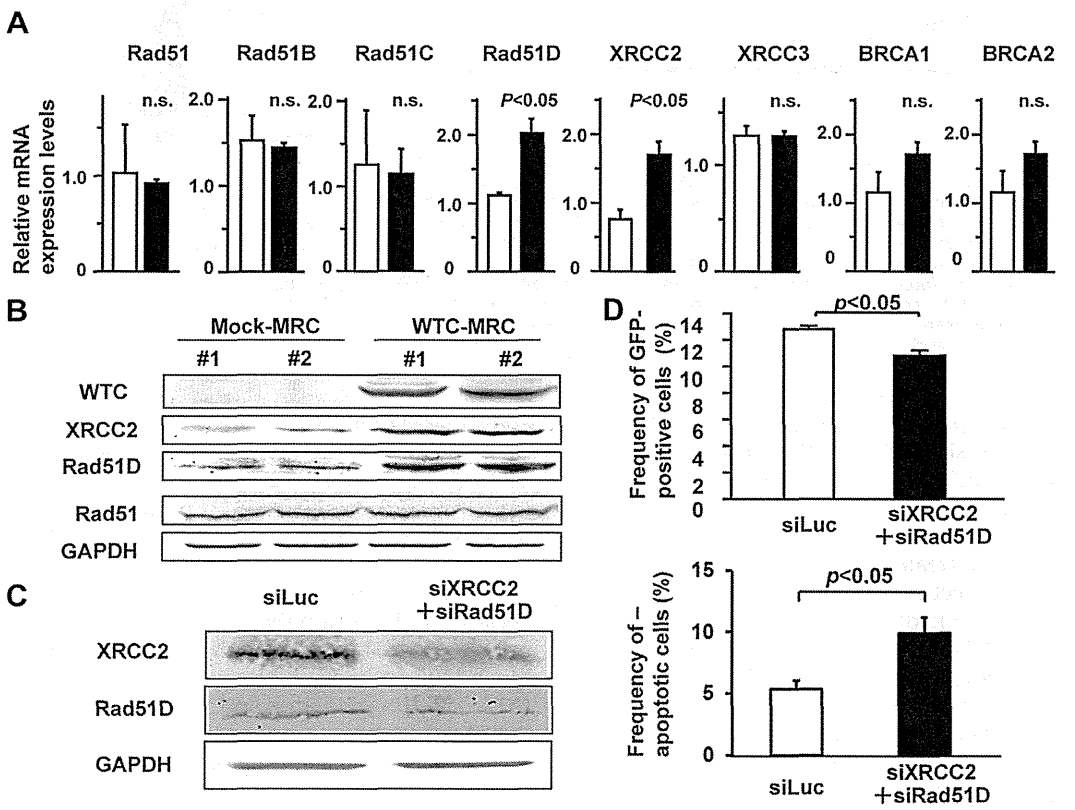

Figure 3. WTC upregulates expression of XRCC2 and Rad51D (early stage genes of HR). (A) Relative mRNA expression levels of HR genes that were involved in early steps of HR were examined by real-time RT-PCR in WTC-MRC and Mock-MRC cells. Expression levels of individual gene in K562 cells were defined as 1.0. (B) Western blot showing increased expression of XRCC2 and Rad51D in cells with forced expression of WTC isoform. (C) Representative Western blot showing knockdown of XRCC2 and Rad51D proteins by transfection with siRNAs. (D) Cells were transfected with both of the XRCC2- and Rad51D-targeting siRNAs (siXRCC2 and siRad51D, respectively) or with control siRNA (siLuc). The cells were introduced with pCBAS vector to generate DSB and incubated for 48 h (upper) and treated with DOX for 24 h (lower). HR-mediated GFP expression (upper) and frequency of apoptotic cells (lower) were determined by flowcytometry. Results were obtained from three independent experiments. Columns, means of frequencies (%) of GFP-positive cells (upper) and annexin V-positive apoptotic cells (lower). Bars, SE.

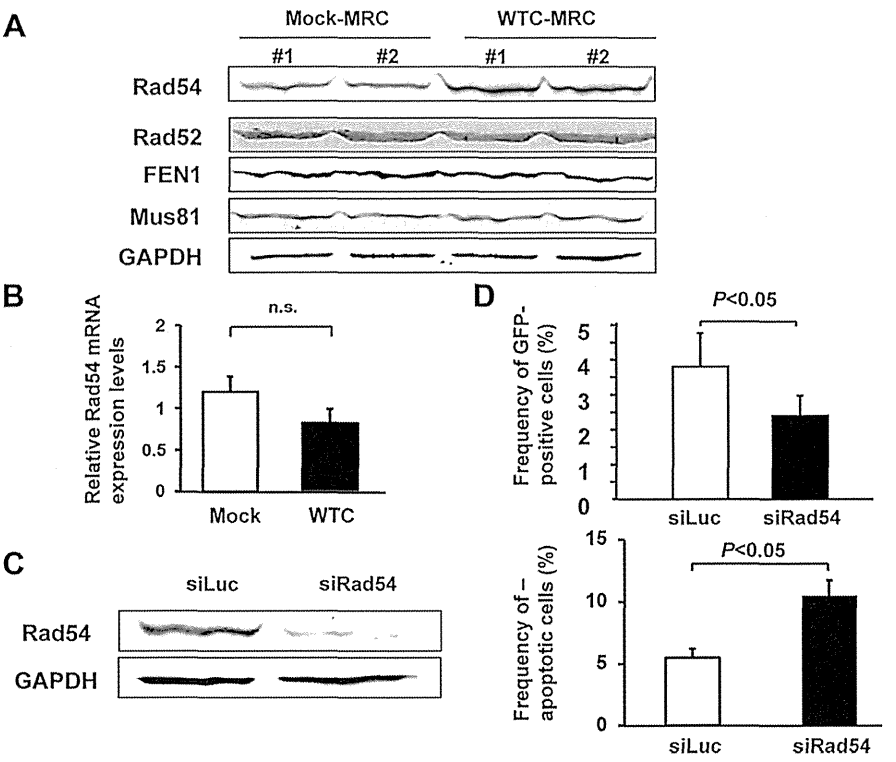

Figure 4. WTC upregulates expression of Rad54 (late stage gene of HR). (A) Western blot showing increased expression of Rad54 in the cells with forced expression of WTC isoform (WTC-MRC cells). (B) Relative Rad54 mRNA expression levels. Mock and WTC indicate Mock- and WTC-MRC cells, respectively. (C) Representative Western blot showing knockdown of Rad54 protein by the siRNA. (D) Cells were transfected with Rad54-targeting siRNAs (siRad54) or with control siRNA (siLuc). The cells were introduced with pCBAS vector to generate DSB and incubated for 48 h (upper) and treated with DOX for 24 h (lower). HR-mediated GFP expression (upper) and frequency of apoptotic cells (lower) was determined by flowcytometry. Results were obtained from three independent experiments. Columns, means of frequencies (%) of GFP-positive cells (upper) and annexin V-positive apoptotic cells (lower). Bars, SE.

transduced by pCBAS vector (Figure 4C). Flowcytometric analysis showed that HR-mediated expression of GFP was significantly suppressed by knockdown of Rad54 (Figure 4D). To examine the involvement of Rad54 in resistance to DOX induced by WTC, WTC-MRC cells were treated with DOX for 24 h two days after the transfection with siRNA targeting Rad54. Knockdown of Rad54 significantly canceled the resistance to DOX in WTC-MRC cells (Figure 4D).

Taken together, these results indicated that WTC isoform alone increased expression of HR genes such as XRCC2, Rad51D, and Rad54 and promoted HR, resulting in acquisition of resistance to DNA-damaging chemotherapeutic agents.

WTC Isoform Protein Directly Binds to XRCC2 and Rad51D Promoters

Chromatin immunoprecipitation (ChIP) assay was performed to examine whether or not WTC isoform protein could directly bind to promoter regions of XRCC2 and Rad51D genes. Although there was no previous report of WT1(KTS+) isoform-binding sequence ($AN_6GGGATGCGGAN_{13}CCN$) (38) of XRCC2 and Rad51D promoters, there were two EWS(KTS+)RE sites [GGAGG(A/G)] (39) in XRCC2 promoter (X1, +346 to +351 and X2, +364 to +369) and five EWS(KTS+)RE sites in Rad51D promoter (R1, −1346 to −1341; R2, −1041 to −1036; R3,−666 to −661; R4,−515 to −510; and R5, +176 to +181) (Figure 5A).

ChIP assay was not performed for Rad54 promoter because no significant increase was observed in Rad54 mRNA expression in WTC-MRC cells compared to Mock-MRC cells and because there was no WT1 (KTS+) binding sequence and no EWS(KTS+)RE site in Rad54 promoter.

Cross-linked chromatins of WTC-MRC cells were immunoprecipitated using one each of WT1 Ab, AcH3 Ab, and non-immune rabbit IgG after sonication. Immunoprecipitated DNA was amplified by real-time PCR using primer pairs jumping X1 and X2 (X1–X2), R1, R2, R3, R4, and R5 regions. Real-time PCR showed neither immunoprecipitation with WT1 Ab nor that with AcH3 Ab enriched R1 promoter region of Rad51D compared to non-immune IgG, which enabled us to use this R1 region as a negative control for binding of WTC protein and Histone3 acetylation.

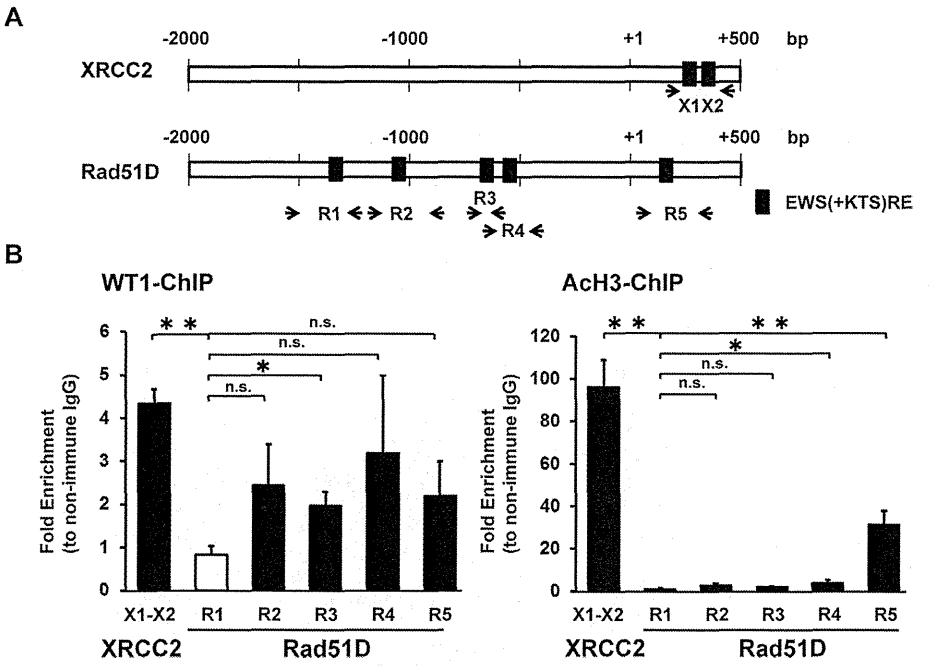

Figure 5. WTC isoform protein directly binds to XRCC2 and Rad51D promoters. (A) localization of EWS(+KTS)RE sequence in XRCC2 and Rad51D promoters. Arrows indicate the PCR primer pairs for amplification of immunoprecipitated genome DNA. (B) ChIP assay. Genomic DNA extracted from WTC-MRC cells was precipitated with WT1 Ab, AcH3 Ab or non-immune IgG. Precipitated DNA was quantified by real-time PCR. Fold enrichment relative to non-immune IgG was calculated for WT1- and AcH3-immunoprecipitated samples by delta Ct method: Fold enrichment = 2^[(Ct-IgG) − −(Ct-WT1) or (Ct-AcH3)]. *$P < 0.05$; **$P < 0.01$.

In WT1-ChIP assay, X1-X2 promoter region of XRCC2 and R3 promoter region of Rad51D were 4.3-fold ($P < 0.001$) and 2.0-fold ($P = 0.025$) enriched, respectively, by immunoprecipitation with WT1 Ab. R2, R4, and R5 promoter regions of Rad51D promoter seemed enriched by immunoprecipitation with WT1 Ab but the difference was not statistically significant. As for AcH3 ChIP analysis, X1-X2 region of XRCC2 and R4 and R5 regions of Rad51D were significantly enriched by immunoprecipitation with AcH3 Ab.

These results indicate that WTC isoform protein directly bound to XRCC2 and Rad51D promoters in WTC-MRC cells.

XRCC2 and Rad54 are Overexpressed in Lung and Gastric Cancers

In the present study, HR factors, Rad54, XRCC2, and Rad51D were shown to be upregulated by WTC isoform. Although overexpression of WT1 protein has been reported in the majority of various types of cancers, expression of these HR factors in cancer cells remains undetermined. Therefore, XRCC2 and Rad54 that were involved in early and mid to late HR process, respectively, were immunohistochemically analyzed for their protein expression in 44 non-small-cell lung and 15 gastric cancers (Figure 6). Both Rad54 and XRCC2 protein was diffusely expressed in the majority of the cases examined. Rad54 protein expression was detected in 39 (89.0%) of 44 NSCLCs and 10 (66.7%) of 15 gastric cancers. XRCC2 protein expression was detected in 36 (82.0%) of 44 NSCLCs and 10 (66.7%) of 15 gastric cancers. Furthermore, correlation of WT1 protein expression with either XRCC2 or Rad54 protein expression was analyzed in NSCLC cases. Expression of both Rad54 and XRCC2 proteins in tumor cells was significantly correlated with that of WT1 protein in these cases (Table 1).

To confirm the correlation of WT1 protein expression with either XRCC2 or Rad54 protein expression in lung cancer cells, Rad54-WT1 and XRCC2-WT1 double staining immunohistochemical studies were further performed using tissue microarray containing 59 NSCLC tissues (Figure 7). As it was difficult to distinguish weakly positive expression from negative one as a result of the increase in staining background by double staining, the protein expression was scored as positive (distinctly stronger staining of cancer cells compared to adjacent regions) or low-negative (weak or negative staining of cancer cells compared to adjacent regions) in double staining. In Rad54-WT1 double staining, 38 (64.4%) and 13 (22.0%) cases of 59 cases were scored as double-positive and double-low-negative, respectively (Figure 7B). In XRCC2-WT1 double staining, 40 (67.8%) and 12 (20.3%) cases of 59 cases were scored as double-positive and double-low-negative, respectively (Figure 7B). These results confirmed the correlation of

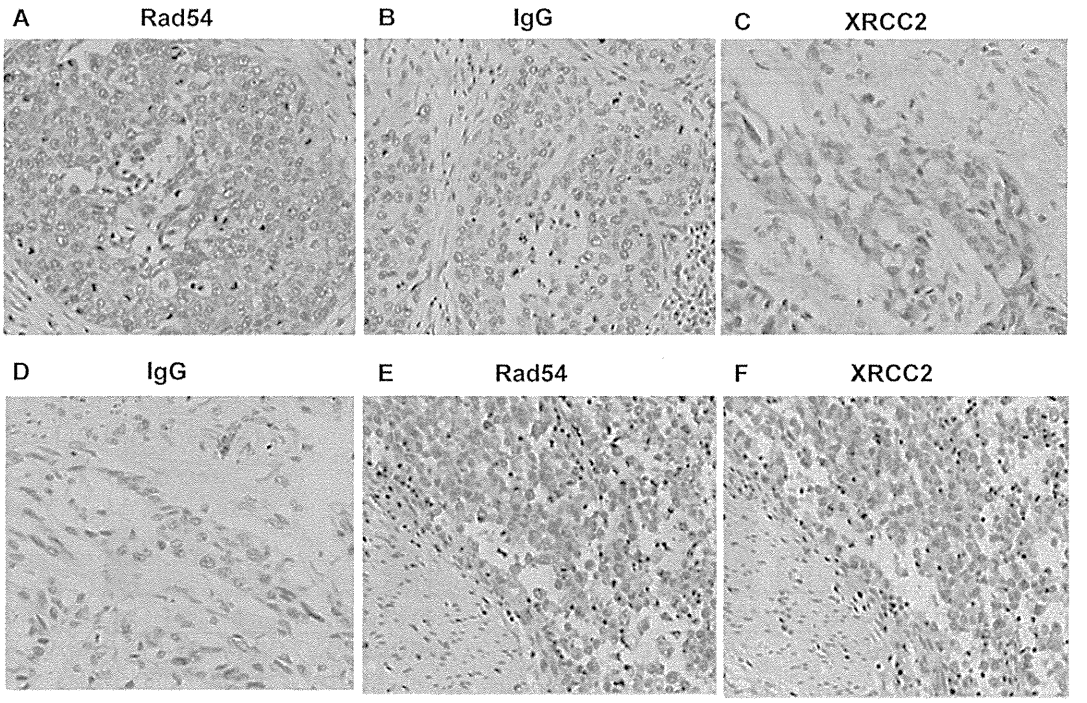

Figure 6. High expression of Rad54 and XRCC2 proteins in non-small-cell-lung and gastric cancer. Representative results of immunohistochemical study of single staining. Staining with Rad54 Ab (A), non-immune IgG (B, D), and XRCC2 Ab (C) in NSCLC, and staining with Rad54 Ab (E) and XRCC2 Ab (F) in gastric cancer are shown. Rad54 and XRCC2 proteins are stained in brown.

WT1 protein expression with either XRCC2 or Rad54 protein expression in lung cancer cells. Similar to the results with NSCLC cases, the correlation of WT1 protein expression with XRCC2 and Rad54 protein expression was observed in gastric cancers (Figure 7C).

Furthermore, co-expression of essential HR factor, Rad51 and WT1 was examined in NSCLC cases. In Rad51-WT1 double staining, 37 (62.7%) and 13 (13.6%) cases of 59 cases were scored as double-positive and double-low-negative, respectively (Figure 6D), suggesting weaker correlation of WT1 protein expression with Rad51 protein expression compared to that with Rad54 or XRCC2 protein in NSCLC cases.

Taken together, XRCC2 and Rad54 are overexpressed in NSCLC and gastric cancers and their expression was correlated with that of WT1 protein in NSCLC.

Table 1. Correlation Between WT1 Expression and Expression of HR-Related Gene Proteins in Non-Small-Cell Lung Cancers

WT1	Positive	Negative	Total	*P-value*
XRCC2				
Positive	33	4	37	
Negative	3	4	7	0.001
Total	36	8	44	
Rad54				
Positive	33	4	37	
Negative	6	1	7	0.001
Total	39	5	44	

Expression of WT1, XRCC2, and Rad54 proteins were immunohistochemically analyzed in non-small-cell lung cancers. Correlation between expression of WT1 protein in tumor cells and homologous recombination-related gene proteins in tumor cells was analyzed using Spearman's correlation coefficient by rank test.

DISCUSSION

Here we showed for the first time that WTC isoform promoted homologous recombination (HR)-mediated DNA damage repair through upregulation of expression of HR factors such as XRCC2, Rad51D, and Rad54. HR-mediated DNA damage repair has been regarded as a mechanism by which genome instability is inhibited and plays a tumor suppressive role. However, our present results showed that enhancement of HR-mediated DNA damage repair enabled cells to acquire resistance to DNA-damaging chemotherapeutic agents as a result of increased repair activity for DNA damage by the agents. The DNA-damaging agents such as DOX, CPT, and MMC used here induced DNA double strand breaks. As HR plays a major role in DNA double strand break repair,

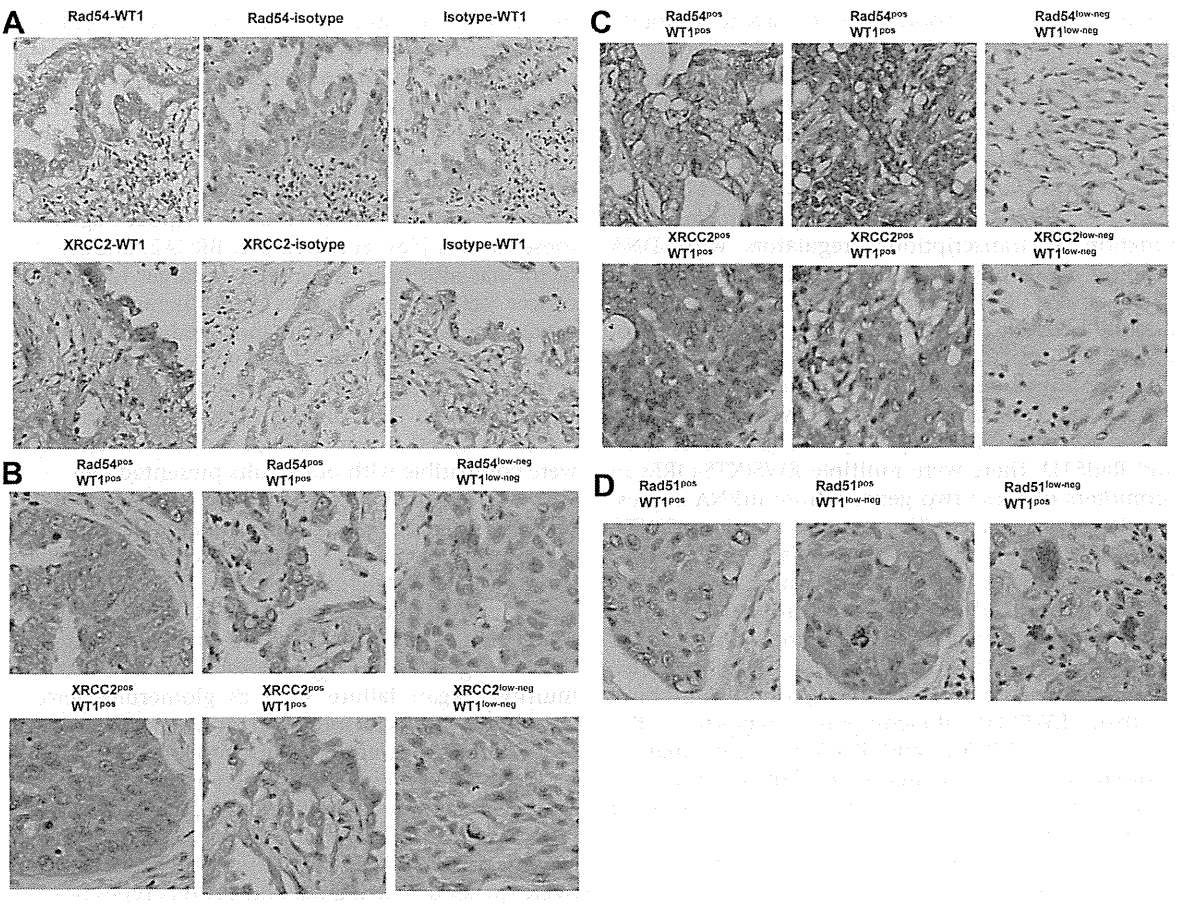

Figure 7. Co-expression of WT1 protein with HR factor proteins. (A) Rad54-WT1 and XRCC2-WT1 double staining immunohistochemical study. (B) Co-expression of WT1 protein with either Rad54 or XRCC2 protein in NSCLC. (C) Co-expression of WT1 protein with either Rad54 or XRCC2 protein in gastric cancer. (D) Representative results of Rad51-WT1 double staining immunohistochemical study in NSCLC. (A–D) Rad54, XRCC2, and Rad51 proteins are stained in brown. WT1 protein is stained in red. The protein expression was scored as positive (distinctly stronger staining of cancer cells compared to adjacent regions) or low-negative (weak or negative staining of cancer cells compared to adjacent regions) in double staining.

it is reasonable that WTC isoform induced resistance (chemoresistance) to these DNA-damaging agents through promotion of HR-mediated repair for DNA double strand break, which is supported by the findings shown in the present study that knockdown of HR factors upregulated by WTC isoform inhibited the increased HR activity and canceled the resistance to DOX in cells with forced expression of WTC isoform. Furthermore, recent evidence has shown that the HR machinery plays a role in replication maintenance through its replication fork-stabilization and fork-restart functions at arrested forks [40]. As the DNA-damaging agents used here are known to primarily induce replication fork stalling as their action mechanism to damage DNA [41–43], one of the mechanisms by which resistance to DNA-damaging agents by WTC isoform was induced may be promotion of replication maintenance through enhanced HR.

Taken together, WTC isoform promotes HR, resulting in acquisition of chemoresisitance of WT1-expressing cancer cells.

In the present study, it was shown that, although the difference was not statistically significant ($P = 0.06$), forced expression of WTC isoform slightly decreased the frequency of cells in S phase of the cell cycle that was the target of most of DNA-damaging agents. Previous reports had shown that XRCC2-defective hamster cells displayed a reduction in the ratio of replication fork progression [44] and that Rad51D-null CHO cells showed reduced growth rate [45], suggesting the involvement of these HR factors in the progression of S phase of the cell cycle. These findings may support a possibility that HR factors XRCC2 and Rad51D upregulated by WTC isoform promote the S phase progression and shorten the S phase, resulting in the decrease in S phase cell population and increase in G2/M phase cell

population under conditions of asynchronously growth without DNA-damaging agents.

WT1(KTS−) isoforms have been well characterized as transcription regulators and their consensus motifs have been identified in the promoters of target genes. These include GC-rich [46], TC repeats [47], WRE [48], and WTE [5] sequences. In contrast to WT1(KTS−) isoforms, whether or not WT1(KTS+) isoforms could function as transcriptional regulators with DNA binding specificity had been undetermined until Wells et al. [38] reported that WT1(KTS+) isoforms directly bound to and transactivate the promoter of planar cell polarity gene *Scribble* in renal podocytes. They identified a responsive element of WT1(KTS+) isoforms and named the sequence as WKE. Although there was no WKE in the promoters of XRCC2 and Rad51D, there were multiple EWS(KTS+)REs in promoters of these two genes whose mRNA expression levels were elevated by forced expression of WTC isoform (17AA−/KTS+) in MRC cells. As EWS(KTS+) RE was identified as a responsive element of the fusion gene that consisted of the transactivational domain of the *EWS* gene and the three C-terminal zinc fingers of the *WT1* gene that retained KTS splice [39], we examined whether WTC isoform protein could bind to these EWS(KTS+)RE-containing regions in the promoters of XRCC2 and Rad51D. ChIP analysis showed that WTC protein bound to the promoters of both genes. Our current results may indicate a possibility that WTC protein directly bound to and transactivate the promoters of XRCC2 and Rad51D. Taken together with the report of Wells et al. [38], it is likely that there are more genes that can be transactivated by WT1(KTS+) isoforms. These genes should be identified for the better understanding of the functions of WT1(KTS+) isoforms that were dominantly expressed in leukemia [27,33] and various types of solid cancers [16,19,20].

Contrary to the important role of HR in the maintenance of genome integrity, HR induces genomic instability under a certain circumstance. As mammalian genomes comprise at least 50% repetitive sequences, HR between repetitive sequences, such as Alu elements can be a significant cause of duplications and deletions of the genome [49]. Furthermore, the HR machinery induces genome instability because fork restart mediated by HR is error-prone [50]. Therefore, HR has two opposite functions: maintenance of genome integrity and induction of genome instability. WTC isoform should be involved in both the acquisition of resistance to DNA-damaging agents of cancer cells through the function of genome integrity maintenance and leukemogensis and tumorigenesis through its functions of genome instability induction.

In the present study, we showed that HR factors, XRCC2 and Rad54 proteins were highly expressed in the majority of NSCLCs and gastric cancers, and there was a significant correlation between expression levels of the HR factors and WT1 protein in NSCLCs. It has been reported that Rad51, an essential HR factor was overexpressed in the majority of pancreatic ductal cancer [51] and that the high expression was associated with unfavorable prognosis in NSCLC [52], esophageal squamous cell carcinoma [53], and colorectal adenocarcinoma [54], Thus, Rad51 can be a target molecule to sensitize tumor cells to chemotherapeutic agents in these tumors [55]. Furthermore, BRCA2, another HR factor has also been reported as a target to sensitize cancer cells to irradiation and chemotherapeutic agents [56,57]. These results indicated that enhanced expression of HR factors such as Rad51 and BRCA2 contributed to the acquisition of chemoresistance of cancer cells to DNA-damaging agents (chemo- and radio-therapies) in various types of solid tumors and were compatible with our results presented here.

The *WT1* gene is physiologically expressed in stem/progenitor cells in various types of organs. In human hematopoietic system, 1.2% of $CD34^+$ hematopoietic stem/progenitor cells expressed the *WT1* gene at high levels comparable to those in K562 leukemia cells [58]. Chau et al. showed that conditional deletion of the *WT1* gene in young and adult mice resulted in multiple organ failure such as glomerulosclerosis, atrophy of the exocrine pancreas and spleen, severe reduction in bone and fat, and failure of erythropoiesis [59]. These results indicated that WT1 played an important role in proliferation and physiological homeostasis of stem/progenitor cells in various organs. It is well known that wild-type *WT1* gene is overexpressed in leukemia and various types of solid tumors. This finding raises the possibility that leukemia and solid tumor cells may be malignant counterparts of WT1-expressing stem/progenitor cells in various organs. In this case, WT1 expression contributes to genome integrity in stem/progenitor cells and simultaneously gives rise to genome instability, resulting in malignant transformation of stem/progenitor cells.

ACKNOWLEDGMENTS

pDR-GFP vector construct was kindly given from Dr Maria Jasin. This work was supported in part by a Grant-in Aid from the Ministry of Education, Science, Sports, Culture, Japan and Technology and the Ministry of Health, Labour, and Welfare, Japan.

REFERENCES

1. Bouwman P, Jonkers J. The effects of deregulated DNA damage signalling on cancer chemotherapy response and resistance. Nat Rev Cancer 2012;12:587–598.
2. Gashler AL, Bonthron DT, Madden SL. Rauscher FJ 3rd, Collins T, Sukhatme VP. Human platelet-derived growth factor A chain is transcriptionally repressed by the Wilms tumor suppressor WT1. Proc Natl Acad Sci USA 1992;89: 10984–10988.
3. Drummond IA, Madden SL, Rohwer-Nutter P, Bell GI, Sukhatme VP. Rauscher FJ 3rd. Repression of the insulin-like growth factor II gene by the Wilms tumor suppressor WT1. Science 1992;257:674–678.

4. Werner H, Re GG, Drummond IA, et al. Increased expression of the insulin-like growth factor I receptor gene, IGF1R, in Wilms tumor is correlated with modulation of IGF1R promoter activity by the WT1 Wilms tumor gene product. Proc Natl Acad Sci USA 1993;90:5828–5832.
5. Lee SB, Huang K, Palmer R, et al. The Wilms tumor suppressor WT1 encodes a transcriptional activator of amphiregulin. Cell 1999;98:663–673.
6. Amin EM, Oltean S, Hua J, et al. WT1 mutants reveal SRPK1 to be a downstream angiogenesis target by altering VEGF splicing. Cancer Cell 2011;20:768–780.
7. Larsson SH, Charlieu JP, Miyagawa K, et al. Subnuclear localization of WT1 in splicing or transcription factor domains is regulated by alternative splicing. Cell 1995;81:391–401.
8. Caricasole A, Duarte A, Larsson SH, et al. RNA binding by the Wilms tumor suppressor zinc finger proteins. Proc Natl Acad Sci USA 1996;93:7562–7566.
9. Call KM, Glaser TM, Ito CY, et al. Isolation and characterization of a zinc finger polypeptide gene at the human chromosome 11 Wilms' tumor locus. Cell 2000;60:509–520.
10. Inoue K, Sugiyama H, Ogawa H, et al. WT1 as a new prognostic factor and a new marker for the detection of minimal residual disease in acute leukemia. Blood 1994; 84:3071–3079.
11. Oji Y, Miyoshi S, Maeda H, et al. Overexpression of the Wilms' tumor gene WT1 in de novo lung cancers. Int J Cancer 2002;100:297–303.
12. Oji Y, Yamamoto H, Nomura M, et al. Overexpression of the Wilms' tumor gene WT1 in colorectal adenocarcinoma. Cancer Sci 2003;94:712–717.
13. Loeb DM, Evron E, Patel CB, et al. Wilms' tumor suppressor gene (WT1) is expressed in primary breast tumors despite tumor-specific promoter methylation. Cancer Res 2001;61: 921–925.
14. Miyoshi Y, Ando A, Egawa C, et al. High expression of Wilms' tumor suppressor gene predicts poor prognosis in breast cancer patients. Clin Cancer Res 2002;8:1167–1171.
15. Nakatsuka SI, Oji Y, Horiuchi T, et al. Immunohistrochemical detection of WT1 protein in a variety of cancer cells. Mod Pathol 2006;19:804–814.
16. Oji Y, Inohara H, Nakazawa M, et al. Overexpression of the Wilms' tumor gene WT1 in head and neck squamous cell carcinoma. Cancer Sci 2003;94:523–529.
17. Oji Y, Nakamori S, Fujikawa M, et al. Overexpression of the Wilms' tumor gene WT1 in pancreatic ductal adenocarcinoma. Cancer Sci 2004;95:583–587.
18. Oji Y, Suzuki T, Nakano Y, et al. Overexpression of the Wilms' tumor gene WT1 in primary astrocytic tumors. Cancer Sci 2004;95:822–827.
19. Ueda T, Oji Y, Naka N, et al. Overexpression of the Wilms' tumor gene WT1 in human bone and soft-tissue sarcomas. Cancer Sci 2003;94:271–276.
20. Wagner N, Panelos J, Massi D, et al. The Wilms' tumor suppressor WT1 is associated with melanoma proliferation. Pflugers Arch 2008;455:839–847.
21. Sotobori T, Ueda T, Oji Y, et al. Prognostic significance of Wilms tumor gene (WT1) mRNA expression in soft tissue sarcoma. Cancer 2006;106:2233–2240.
22. Algar EM, Khromykh T, Smith SI, Blackburn DM, Bryson GJ, Smith PJ. A WT1 antisense oligonucleotide inhibits proliferation and induces apoptosis in myeloid leukaemia cell lines. Oncogene 1996;12:1005–1014.
23. Yamagami T, Ogawa H, Tamaki H, et al. Suppression of Wilms' tumor gene (WT1) expression induces G2/M arrest in leukemic cells. Leuk Res 1998;22:383–384.
24. Inoue K, Tamaki H, Ogawa H, et al. Wilms' tumor gene (WT1) competes with differentiation-inducing signal in hematopoietic progenitor cells. Blood 1998;91:2969–2976.
25. Tsuboi A, Oka Y, Ogawa H, et al. Constitutive expression of the Wilms' tumor gene WT1 inhibits the differentiation of myeloid progenitor cells but promotes their proliferation in response to granulocyte-colony stimulating factor (G-CSF). Leuk Res 1999;23:499–505.
26. Jomgeow T, Oji Y, Tsuiji N, et al. Wilms' tumor gene WT1 17AA(−)/KTS(−) isoform induces morphological changes and promotes cell migration and invasion in vitro. Cancer Sci 2006;97:259–270.
27. Ito K, Oji Y, Tatsumi N, et al. Antiapoptotic function of 17AA(+)WT1 (Wilms' tumor gene) isoforms on the intrinsic apoptosis pathway. Oncogene 2006;25:4217–4229.
28. Tatsumi N, Oji Y, Tsuji N, et al. Wilms' tumor gene WT1-shRNA as a potent apoptosis-inducing agent for solid tumors. Int J Oncol 2008;32:701–711.
29. Wagner KD, Wagner N, Wellmann S, et al. Oxygen-regulated expression of the Wilms' tumor suppressor Wt1 involves hypoxia-inducible factor-1 (HIF-1). FASEB J 2003;17:1364–1366.
30. McCarty G, Awad O, Loeb DM. WT1 protein directly regulates expression of vascular endothelial growth factor and is a mediator of tumor response to hypoxia. J Biol Chem 2011;286:43634–43643.
31. Wagner N, Michiels JF, Schedl A, Wagner KD. The Wilms' tumour suppressor WT1 is involved in endothelial cell proliferation and migration: Expression in tumour vessels in vivo. Oncogene 2008;27:3662–3672.
32. Bourkoula K, Englert C, Giaisi M, Köhler R, Krammer PH, Li-Weber M. The Wilms' tumor suppressor WT1 enhances CD95L expression and promotes activation-induced cell death in leukemic T cells. Int J Cancer 2014;134:291–300.
33. Kramarzova K, Stuchly J, Willasch A, et al. Real-time PCR quantification of major Wilms' tumor gene 1 (WT1) isoforms in acute myeloid leukemia, their characteristic expression patterns and possible functional consequences. Leukemia 2012;26:2086–2095.
34. Pierce AJ, Johnson RD, Thompson LH, Jasin M. XRCC3 promotes homology-directed repair of DNA damage in mammalian cells. Genes Dev 1999;13:2633–2638.
35. Sakamoto S, Iijima K, Mochizuki D, et al. Homologous recombination repair is regulated by domains at the N- and C-terminus of NBS1 and is dissociated with ATM functions. Oncogene 2007;26:6002–6009.
36. Lan HY, Mu W, Nikolic-Paterson DJ, et al. A novel, simple, reliable, and sensitive method for multiple immunoenzyme staining: Use of microwave oven heating to block antibody crossreactivity and retrieve antigens. J Histochem Cytochem 1995;43:97–102.
37. Kurumizaka H, Ikawa S, Nakada M, et al. Homologous pairing and ring and filament structure formation activities of the human Xrcc2-Rad51D complex. J Biol Chem 2002;277: 14315–14320.
38. Wells J, Rivera MN, Kim WJ, et al. The predominant WT1 isoform (+KTS) encodes a DNA-binding protein targeting the planar cell polarity gene Scribble in renal podocytes. Mol Cancer Res 2010;8:975–985.
39. Reynolds PA, Smolen GA, Palmer RE, et al. Identification of a DNA-binding site and transcriptional target for the EWS-WT1 (+KTS) oncoprotein. Genes Dev 2003;17:2094–2107.
40. Costes A, Lambert SAE. Homologous recombination as a replication fork escort: Fork-protection and recovery. Biomolecules 2013;3:39–71.
41. Thorn CF, Oshiro C, Marsh S, et al. Doxorubicin pathways: Pharmacodynamics and adverse effects. Pharmacogenet Genomics 2011;21:440–446.
42. Pommier Y. Topoisomerase I inhibitors: Camptothecins and beyond. Nat Rev Cancer 2006;6:789–802.
43. Mladenov E, Tsaneva I, Anachkova B. Activation of the S phase DNA damage checkpoint by mitomycin C. J Cell Physiol 2007;211:468–476.
44. Daboussi F, Courbet S, Benhamou S, et al. A homologous recombination defect affects replication-fork progression in mammalian cells. J Cell Sci 2008;121:162–166.

45. Urbin SS, Elvers I, Hinz JM, et al. Uncoupling of RAD51 focus formation and cell survival after replication fork stalling in RAD51D null CHO cells. Environ Mol Mutagen 2012;53:114–124.
46. Rauscher FJ 3rd, Morris JF, Tournay OE, et al. Binding of the Wilms' tumor locus zinc finger protein to the EGR-1 consensus sequence. Science 1990;250:1259–1262.
47. Wang ZY, Qiu QQ, Enger KT, Deuel TF. A second transcriptionally active DNA-binding site for the Wilms tumor gene product, WT1. Proc Natl Acad Sci USA 1993;90:8896–8900.
48. Nakagama H, Heinrich G, Pelletier J, Housman DE. Sequence and structural requirements for high-affinity DNA binding by the WT1 gene product. Mol Cell Biol 1995;15:1489–1498.
49. Ade C, Roy-Engel AW, Deininger PL. Alu elements: An intrinsic source of human genome instability. Curr Opin Virol 2013;3:639–645.
50. Carr AM, Lambert S. Replication stress-induced genome instability: The dark side of replication maintenance by homologous recombination. J Mol Biol 2013;425:4733–4744.
51. Maacke H, Jost K, Opitz S, et al. DNA repair and recombination factor Rad51 is over-expressed in human pancreatic adenocarcinoma. Oncogene 2000;19:2791–2795.
52. Qiao GB, Wu YL, Yang XN, et al. High-level expression of Rad51 is an independent prognostic marker of survival in non-small-cell lung cancer patients. Br J Cancer 2005;93:137–143.
53. Li Y, Yu H, Luo RZ, et al. Elevated expression of Rad51 is correlated with decreased survival in resectable esophageal squamous cell carcinoma. J Surg Oncol 2011;104:617–622.
54. Tennstedt P, Fresow R, Simon R, et al. RAD51 overexpression is a negative prognostic marker for colorectal adenocarcinoma. Int J Cancer 2013;132:2118–2126.
55. Nogueira A, Assis J, Catarino R, Medeiros R. DNA repair and cytotoxic drugs: The potential role of RAD51 in clinical outcome of non-small-cell lung cancer patients. Pharmacogenomics 2013;14:689–700.
56. Yu D, Sekine E, Fujimori A, Ochiya T, Okayasu R. Down regulation of BRCA2 causes radio-sensitization of human tumor cells in vitro and in vivo. Cancer Sci 2008;99:810–815.
57. Quiros S, Roos WP, Kaina B. Rad51 and BRCA2–New molecular targets for sensitizing glioma cells to alkylating anticancer drugs. PLoS ONE 2011;6:e27183.
58. Hosen N, Sonoda Y, Oji Y, et al. Very low frequencies of human normal $CD34^+$ haematopoietic progenitor cells express the Wilms' tumour gene WT1 at levels similar to those in leukaemia cells. Br J Haematol 2002;116:409–420.
59. Chau YY, Brownstein D, Mjoseng H, et al. Acute multiple organ failure in adult mice deleted for the developmental regulator Wt1. PLoS Genet 2011;7:e1002404.